Published in final edited form as:
Biochemistry. 2011 December 27; 50(51): 11143–11161. doi:10.1021/bi201636s.

Phosphatidylinositol (3,4,5)-Trisphosphate Activity Probes for the Labeling and Proteomic Characterization of Protein Binding Partners

Meng M. Rowland[†], **Heidi E. Bostic**[†], **Denghuang Gong**[†], **Anna E. Speers**[§], **Nathan Lucas**[‡], **Wonhwa Cho**[‡], **Benjamin F. Cravatt**[§], and **Michael D. Best**[†,*]

[†]Department of Chemistry, the University of Tennessee 1420 Circle Drive, Knoxville, TN 37996

[§]The Skaggs Institute for Chemical Biology and Department of Chemical Physiology, The Scripps Research Institute, La Jolla, CA 92037, USA

[‡]Department of Chemistry, the University of Illinois at Chicago 845 West Taylor Street, Chicago, IL 60607-7061

Abstract

Phosphatidylinositol polyphosphate lipids, such as phosphatidylinositol (3,4,5)-trisphosphate ($PI(3,4,5)P_3$), regulate critical biological processes, many of which are aberrant in disease. These lipids often act as site-specific ligands in interactions that enforce membrane-association of protein binding partners. Herein, we describe the development of bifunctional activity probes corresponding to the headgroup of $PI(3,4,5)P_3$ that are effective for identifying and characterizing protein binding partners from complex samples, namely cancer cell extracts. These probes contain both a photoaffinity tag for covalent labeling of target proteins as well as a secondary handle for subsequent detection or manipulation of labeled proteins. Probes bearing different secondary tags were exploited, either by direct attachment of a fluorescent dye for optical detection or by using an alkyne that can be derivatized after protein labeling via click chemistry. First, we describe the design and modular synthetic strategy used to generate multiple probes with different reporter tags of use for characterizing probe-labeled proteins. Next, we report initial labeling studies using purified protein, the PH domain of Akt, in which probes were found to label this target, as judged by on-gel detection. Furthermore, protein labeling was abrogated by controls including competition with an unlabeled $PI(3,4,5)P_3$ headgroup analog as well as through protein denaturation, indicating specific labeling. In addition, probes featuring different linker lengths between the $PI(3,4,5)P_3$ headgroup and photoaffinity tag led to variations in protein labeling, indicating that a shorter linker was more effective in this case. Finally, proteomic labeling studies were performed using cell extracts, labeled proteins were observed by in-gel detection and characterized using post-labeling with biotin, affinity chromatography and identification via tandem mass spectrometry. These studies yielded a total of 265 proteins, including both known and novel candidate $PI(3,4,5)P_3$-binding proteins.

Introduction

The phosphatidylinositol polyphosphates (PIP_ns), also known as the phosphoinositides, represent an important family of signaling lipids that control numerous key cellular

[*]Phone: 865-974-8658, Fax: 865-974-9332, mdbest@utk.edu.

Supplemental Information

Supplemental Information includes procedures, characterization data, and color gel images. This material is available free of charge via the Internet at http://pubs.acs.org.

processes.[1,2] These molecules contained a conserved *myo*-inositol headgroup that is attached via a phosphodiester linkage at the 1-position to a glycerolipid backbone. The family consists of seven naturally occurring isomers that exhibit differential patterns of phosphorylation, specifically including every combination of phosphate groups at the 3, 4, and 5 positions of the *myo*-inositol headgroup. A primary activity of the PIP_ns is to serve as site-specific ligands in protein binding events that enforce protein−membrane association.[3,4] Due to the key roles of these lipids in regulating critical biological pathways, they have been linked to aberrant activities associated with diseases, including cancer and diabetes.[5–8] One of the most prominent links to disease involves the role of phosphatidylinositol (3,4,5)-trisphosphate ($PI(3,4,5)P_3$) as a ligand for Akt (protein kinase B).[9–14] This binding event promotes association of Akt with the inner leaflet of the plasma membrane,[15] where it is then activated through multiple phosphorylation events. Activated Akt feeds into numerous pathways that promote cell survival, and thus the enzymes that produce (phosphoinositide 3-kinase)[16] and hydrolyze (PTEN)[17] $PI(3,4,5)P_3$ are among the most commonly mutated enzymes in cancer.[18,19]

The understanding of PIP_n binding properties is hindered by complexity at multiple levels. Many proteins that bind PIP_ns contain one or more of a number of conserved binding module sequences, such as the PH, PX, FYVE, ENTH, ANTH, FERM, Tubby, and PROPPIN domains, members of which can be identified by sequence homology searches. New domain families have continued to be discovered in recent years and there are likely further as yet undiscovered PIP_n-targeting sequences. Furthermore, complexities often arise within domain families, such as with the PH domains, where only a fraction of family members bind PIP_ns, and those PH-domain containing proteins that do bind PIP_ns exhibit broad diversity in their specificities for particular PIP_n targets. Finally, other proteins that bind PIP_ns appear to lack any consensus binding sequence, making them more difficult to identify. As a result of these complexities, global methods for the identification and characterization of PIP_n-binding proteins are of significant interest.

The primary method that has been effectively employed for global characterization of PIP_n-binding proteins has involved affinity purification using solid supports decorated with different lipid motifs.[20–27] Affinity chromatography using PIP_n-functionalized beads was initially used to purify individual proteins,[28,29] and applications have since expanded due to advancements in the technology for identifying protein binding partners. In an early example, libraries of radiolabeled proteins were screened, which led to the identification of 2 known and 1 new target of different PIP_ns.[20] The scope of studies has expanded due to progress in mass spectrometry-based proteomic analysis, resulting in the identification of numerous PIP_n-binding proteins.[22,24–27,30] In a recent report, 282 $PI(3,4,5)P_3$-binding proteins were identified using beads decorated with this headgroup that were either used directly for studies or through incorporation of the beads into liposomes to better mimic the environment of cellular membranes.[25] In addition to affinity chromatography, proteome chips have also been used to probe protein−PIP_n binding interactions.[31] This was performed by immobilizing GST-tagged proteins from yeast, followed by microarray analysis of binding to biotin-labeled PIP_n-containing liposomes. One note regarding these proteomic analyses is that the exact set of proteins that have been identified has varied among the studies. This indicates that the specific conditions that are employed for analysis affect the results, suggesting that it will be beneficial to pursue diverse approaches to elucidate the full complement of PIP_n-binding proteins.

A strategy that shows great prospects for broad and efficient characterization of lipid-binding proteins is activity-based protein profiling (ABPP),[32] in which protein targets are collectively characterized based on function, in this case ligand binding properties. In this approach, target proteins are collectively labeled, purified and characterized from complex

biological samples such as cell extracts and live cells using small molecule probes that range from active-site directed analogs of enzyme substrates to derivatized versions of biologically active ligands. Recently, phospholipid-based activity probes have been applied to characterize both lipid-binding proteins[33,34] and lipid-modifying phospholipase enzymes[35] using synthetic analogs of phosphatidylcholine. A significant advantage of ABPP is that protein targets can be labeled in living cells, allowing for the probing of activities under normal physiological conditions, which is critical since proteins operate much differently in live cells than in cell extracts. In addition, the covalent labeling of protein targets in ABPP circumvents the problem of non-covalent interactions falling apart during processing, and enhances the likelihood of identifying protein targets that bind the probe with weaker affinities. Due to the benefits of ABPP, we set out to develop activity-based probes corresponding to the PIP_ns that are effective for proteomics towards their eventual use in live cell labeling studies.

Experimental Procedures

General Experimental

Reagents were generally purchased from Acros, Aldrich or Fisher Scientific and used as received. Dry solvents were obtained from a Pure Solv solvent delivery system purchased from Innovative Technology, Inc. Column chromatography was performed using 230–400 mesh silica gel purchased from Sorbent Technologies and C18 (17%) reverse phase column (6 mL, 2 g) purchased from Silicycle. NMR spectra were obtained using a Varian Mercury 300 spectrometer. Mass spectra were obtained with an ABI DE Pro MALDI spectrometer with high-resolution capabilities. Protein photo-cross-linking was performed using a Spectroline ENF260C UV lamp. Proteins were visualized in-gel using a Hibachi FMBio lle flatbed laser-induced fluorescence scanner (MiraiBio, Alameda, CA). Dulbecco's Phosphate-Buffered Saline (PBS) was purchased from Cellgro. Cell lines were purchased from ATCC. Heat-denatured proteins or cell extracts were generated by denaturing at 90°C for 5 minutes. PIP_n headgroup−amine conjugates **4a** and **4b**[36], Azidorhodamine **11**[37], and THPTA[38] were each synthesized according to previously reported procedures. The GST-tagged PH domain of Akt was expressed and purified as previously reported.[39] Cancer cell extracts were prepared using a previously reported procedure.[37]

1. Synthesis of PIP_n activity-based probes

Benzophenone-Lys-OMe (6): A reported procedure[40] was used to prepare compound **6.** Cbz-Lys(Boc)-OMe (**5**) (262 mg, 0.664 mmol) was dissolved in 5 mL methanol. And palladium(II) hydroxide (26 mg, 10% wt) was added to the solution. The reaction was stirred under hydrogen atmosphere overnight, and the reaction crude was then filtered through a pad of cellite. The filtrate was concentrated to yield Lys(Boc)-OMe, which was used in the next step without further purification. Lys(Boc)-OMe was dissolved in 10 mL *N,N*-dimethylformamide, to which was added 4-benzoylbenzoic acid (150 mg, 0.664 mmol), *N*-(3-Dimethylaminopropyl)-*N*′-ethylcarbodiimide hydrochloride (EDCI, 153 mg, 0.797 mmol), 4-(dimethylamino)pyridine (DMAP, 97 mg, 0.791 mmol), *N*-methylmorpholine (NMM, 0.26 mL, 2.32 mmol). The solution was stirred at rt overnight and then concentrated under reduced pressure. The crude was purified by silica gel column chromatography with a solvent system of 50% ethyl acetate / hexanes to yield benzophenone-Lys(Boc)-OMe as a white foam (279 mg, 90% over 2 steps). The characterization of benzophenone-Lys(Boc)-OMe matches with the literature.[40] Benzophenone-Lys(Boc)-OMe (0.279 g, 0.595 mmol) was then dissolved in 4 mL of trifluoroacetic acid / dichloromethane (v/v 1:1). The reaction was allowed to stir at rt for 2 h and was then concentrated under reduced pressure to yield **6** as a yellowish gum (0.272 g, 100%).

^{1}H NMR (300MHz, $CDCl_3$) δ 7.88 (d, *J* = 9Hz, 1H), 7.70-7.67 (m, 4H), 7.57-7.52 (m, 2H), 7.44-7.40 (m, 2H), 4.67-4.65 (m, 1H), 3.66 (s, 3H), 2.89-2.87 (m, 2H), 1.86-1.64 (m, 4H), 1.46-1.43 (m, 2H). ^{13}C NMR (300MHz, $CDCl_3$) δ 196.7, 172.6, 140.7, 136.7, 136.5, 133.4, 130.2, 130.1, 128.7, 127.5, 53.0, 52.8, 40.2, 31.3, 26.7, 22.4. MALDI-HRMS $[M + Na]^+$ calcd for 391.1634; found 391.1632.

Benzophenone-Lys(5(6)-carboxy fluorescein)-OMe (7a): Benzophenone-Lys-OMe (**6**, 175 mg, 0.475 mmol) was combined with 5(6)-carboxyfluorescein (197 mg, 0.522 mmol), *N*-(3-Dimethylaminopropyl)-*N*′-ethylcarbodiimide hydrochloride (EDCI, 118 mg, 0.618 mmol), 4-(dimethylamino)pyridine (DMAP, 70 mg, 0.570 mmol), *N*-methylmorpholine (NMM, 0.21 mL, 1.90 mmol) in 8 mL dry *N*,*N*-dimethylformamide. The reaction was allowed to stir at rt overnight, at which point the solvent was removed under reduced pressure. The crude was dissolved in 50 mL methanol/chloroform (v/v 1:4) and extracted with 50 mL 2N hydrochloric acid aqueous solution, and the aqueous layer was washed 2 × 50 mL methanol/chloroform (v/v 1:4). The organic layers were then combined, dried with magnesium sulfate, concentrated by rotary evaporation, and then purified using column chromatography with a gradient solvent system of 5-10% methanol / chloroform to yield benzophenone-Lys(5(6)-carboxy fluorescein)-OMe (**7a**) as an orange solid (159 mg, 46%).

^{1}H NMR (300MHz, $CD_3OD/CDCl_3$ (v/v 1:2)) δ 8.40-8.39 (m, 1H), 8.03-7.98 (m, 2H), 7.95-7.83 (m, 2H), 7.85-7.75 (m, 3H), 7.66-7.69 (m, 1H), 7.54-7.49 (m, 2H), 7.25-7.22 (m, 1H), 6.72-6.70 (m, 2H), 6.57-6.53 (m, 4H), 4.76-4.72 (m, 1H), 3.80 (s, 3H), 3.50-3.48 (m, 1H), 3.36-3.35 (m, 1H), 2.67 (bs, 1H), 2.06-1.94 (m, 2H), 1.74-1.46 (m, 4H). MALDI-HRMS $[M + Na]^+$ calcd for 749.2111; found 749.2165.

Benzophenone-Lys(5(6)-carboxy fluorescein)-OH (7b): Compound **7a** (36 mg, 0.050 mmol) was suspended in 5 mL of methanol. To this solution was added 5 mL of 2M sodium hydroxide aqueous solution, and the reaction was stirred at rt for 10 min, followed by addition of 30 mL of 2N hydrochloric acid aqueous solution. An orange solid was formed immediately upon addition of the acid, which was filtered and washed with 2 × 10 mL of 2N hydrochloric acid aqueous solution to yield the crude **7b**. The crude was then dissolved in acetonitrile/water and purified on a C18 reverse phase column (2g) with a gradient solvent system of 0–80% acetonitrile/water. Compound **7b** eluted with ~45–60% acetonitrile/water solution. The collected fractions were concentrated by rotary evaporation to remove acetonitrile. The acetonitrile was then removed by rotary evaporation, followed by lyophilization of the water to yield benzophenone-Lys(5(6)-carboxy fluorescein)-OH (**7b**) as a yellow powder (19 mg, 53%).

^{1}H NMR (300MHz, CD_3CN/D_2O (v/v 1:1)) δ 8.73-8.71 (m, 1H), 8.42-8.29 (m, 4H), 8.14-8.07 (m, 4H), 7.92-7.87 (m, 2H), 7.53-7.50 (m, 1H), 7.10 (s, 2H), 6.97-6.93 (m, 4H), 4.95-4.85 (m, 1H), 3.82-3.80 (m, 1H), 3.67-3.65 (m, 1H), 2.40-2.38 (m, 2H), 1.94-1.80 (m, 4H). MALDI-HRMS $[M + H]^+$ calcd for 713.2130; found 713.2072.

Benzophenone-Lys(alkyne)-OMe (8a): Benzophenone-Lys-OMe (**6**) (911 mg, 1.890 mmol) was combined with alkyne **10** (293 mg, 1.89 mmol), *N*-(3-Dimethylaminopropyl)-*N*′-ethylcarbodiimide hydrochloride (EDCI, 543 mg, 2.83 mmol), 4-(dimethylamino)pyridine (DMAP, 346 mg, 2.83 mmol), and *N*-methylmorpholine (NMM, 2.08 mL, 18.9 mmol) in 10 mL of methanol/chloroform (v/v 1:4). The reaction was allowed to stir at rt overnight, and the solvent was then removed under reduced pressure. The crude was purified by column chromatography with a gradient solvent system of 50–100% acetone/hexanes to yield benzophenone-Lys(alkyne)-OMe (**8a**) as a colorless crystal (760 mg, 80%).

^{1}H NMR (300MHz, $CDCl_3$) δ 7.99-7.96 (m, 2H), 7.81-7.75 (m, 3H), 7.61-7.57 (m, 1H), 7.50-7.42 (m, 3H), 6.81-6.79 (m, 1H), 6.55-6.51(m, 1H), 4.74-4.67 (m, 1H), 3.95-3.93 (m, 2H), 3.75 (s, 3H), 3.27-3.15 (m, 2H), 2.42-2.41 (m, 4H), 2.17-2.14 (m, 1H), 1.90-1.86 (m, 2H), 1.53-1.42 (m, 4H). MALDI-HRMS $[M + Na]^+$ calcd for 528.2105; found 528.2134.

Benzophenone-Lys(alkyne)-OH (8b): Compound **8a** (135 mg, 0.267 mmol) was dissolved in a mixture of 10 mL of methanol/ethanol (v/v 1:1). To this solution was added 8 mL of 2M sodium hydroxide aqueous solution. The reaction was stirred at rt for 15 min and was then extracted from 2N hydrochloric acid aqueous solution (100 mL) with 200 mL dichloromethane, and the aqueous layer was washed with 3 × 50 mL of methanol/ chloroform (v/v 1:4). The combined organic layers were then dried with magnesium sulfate, filtered and concentrated to yield benzophenone-Lys(alkyne)-OH (**8b**) as a white solid (94 mg, 72 %).

^{1}H NMR (300MHz, CD_3OD) δ 8.01-7.99 (m, 2H), 7.84-7.76 (m, 4H), 7.65-7.63 (m, 1H), 7.55-7.53 (m, 2H), 4.59-4.57 (m, 1H), 3.95-3.93 (m, 1H), 3.65-3.61 (m, 2H), 3.21-3.19 (m, 2H), 2.57-2.45 (m, 5H), 1.99.92 (m, 2H), 1.56-1.54 (m, 4H). ^{13}C NMR (300MHz, $CDCl_3$) δ 196.2, 174.2, 171.9, 168.0, 140.0, 137.3, 136.8, 132.8, 129.7, 129.6, 128.3, 127.4, 78.2, 71.1, 53.1, 38.9, 30.6, 28.5, 28.2, 23.2, 21.4.MALDI-HRMS $[M + Na]^+$ calcd for 514.1954; found 514.1974.

Benzophenone-Lys(alkyne)-hexanoate (9a): Carboxylic acid **8b** (144 mg, 0.293 mmol) was combined with 5-aminocaproic acid methyl ester hydrochloride (69 mg, 0.381 mmol), *N*-(3-Dimethylaminopropyl)-*N*′-ethylcarbodiimide hydrochloride (EDCI,72 mg, 0.381 mmol), 4-(dimethylamino)pyridine (DMAP, 47 mg, 0.381 mmol), and *N*-methylmorpholine (NMM, 0.32 mL, 2.92 mmol) in 15 mL methanol/chloroform (v/v 1:4). The reaction was allowed to stir at rt overnight, and the solvent was then removed under reduced pressure. The crude was purified by column chromatography with a gradient solvent system of 50–100% acetone/hexanes to yield compound **9a** as a colorless crystal (91 mg, 50%).

^{1}H NMR (300MHz, $CDCl_3$) δ 8.00-7.97 (m, 2H), 7.83-7.77 (m, 4H), 7.64-7.59 (m, 1H), 7.52-7.47 (m, 2H), 7.21-7.19 (m, 1H), 6.83-6.81(m, 1H), 4.68-4.66 (m, 1H), 3.98-3.96 (m, 2H), 3.64 (s, 3H), 3.25-3.23 (m, 4H), 2.54-2.48 (m, 4H), 2.29 (t, J = 6 Hz, 2H), 2.21-2.18 (m, 1H), 1.92-1.83 (m, 2H), 1.62-1.34 (m, 10H). ^{13}C NMR (300MHz, $CDCl_3$) δ 196.1, 174.1, 172.5, 172.4, 171.7, 166.8, 140.3, 136.9, 133.0, 130.1, 130.0, 128.5, 127.4, 79.7, 71.31, 53.7, 51.6, 39.4, 33.8, 31.3, 29.1, 26.3, 24.4, 22.8. MALDI-HRMS $[M + Na]^+$ calcd for 641.2951; found 641.2953.

4-Oxo-4-(2-propyn-1-ylamino) butanoic acid (10).[41]: Propargylamine (1.5 mL, 21.87 mmol) was dissolved in 10 mL of *N*,*N*-dimethylformamide/acetontrile (v/v: 1/1) at 0°C. To this solution was added succinic anhydride (2.19 g, 21.87 mmol) in 10 mL of acetonitrile, and the resulting solution was stirred at rt overnight. Next, the solvent was removed under reduced pressure. The residue was then washed with hexanes and then ethyl ether to obtain crude **10** as a brownish solid. The crude product was purified by column chromatography with 50–75% ethyl acetate/hexanes to yield **10** as a pale yellowish solid (1.414 g, 42%).

^{1}H NMR (300MHz, CD_3OD) δ 3.94 (d, *J* = 3Hz, 1H), 2.61-2.56 (m, 2 H), 2.49-2.44 (m, 2H). ^{13}C NMR (300MHz, $CDCl_3$) δ 174.8, 172.7, 79.2, 70.8, 29.9, 28.7, 28.1. DART-HRMS $[M + H]^+$ calcd for 156.0661; found 156.0670.

Benzophenone-Lys(5(6)carboxy fluorescein)-PI(3,4)P_2 (1): Acid **7b** (28 mg, 0.039 mmol) was dissolved in 4 mL of *N*,*N*-dimethylformamide/tetrahydrofuran (v/v 1:2). To this stirred solution was added dicyclohexylcarbodiimide (DCC, 16 mg, 0.078 mmol) and then *N*-

hydroxysuccinimide (9 mg, 0.078 mmol). The reaction was stirred for 8 h at rt and then filtered. The filtrate was concentrated to ~0.5 mL, to which was added 50 mL of ethyl ether, after which an orange precipitate was formed and filtered. The solid was then dissolved in 10 mL of tetrahudrofuran and filtered. The filtrate was concentrated to yield the NHS ester of **7b**, which was moved to the next step without further purification. The resulting succinimidyl ester was dissolved in 1 mL of *N,N*-dimethylformamide, to which was added amino-tagged to a solution of PI(3,4)P_2−amine **4a**[36] (10 mg, 0.019 mmol) in 1 mL tetraethylammonium bicarbonate (TEAB, 1 M, pH=7.5) and 0.5 mL tetrahydrofuran. The reaction was allowed to stir at rt overnight, and the solvent was then removed under reduced pressure. The solid crude product was washed with acetone (3 × 20 mL) and then dissolved in deionized water to stir with 500 mg chelex 100, sodium form at rt for 2 h. The reaction solution was then directly loaded onto a C18 reverse-phase column (2 g) and the column was eluted with deionized water (20 mL). The water elution was lyophilized to yield **1** as a yellow solid (8.0 mg, 35%).

^{1}H NMR (300MHz, CD_3OD/D_2O (v/v 1:1)) δ 7.75-7.00 (m, 12 H), 6.55 (s, 2 H), 6.30-6.28 (m, 2H), 5.89-5.86 (s, 2 H), 4.30-4.28 (s, 2 H), 4.02-3.98 (m, 2H), 3.72-3.31 (m, 14H), 1.53-1.04 (m, 14H). ^{31}P NMR (121.5 MHz, CD_3OD/D_2O (v/v 1:1)): 5.05, 3.64, 0.12. MALDI-HRMS $[M + H]^+$ calcd for 1214.2696; found 1214.7771.

Benzophenone-Lys(alkyne)-PI(3,4,5)P_3 (2): Acid **9b** (47 mg, 0.096 mmol) was dissolved in 5 mL of tetrahydrofuran. To this stirred solution was added *N*-(3-Dimethylaminopropyl)-*N*′-ethylcarbodiimide hydrochloride (EDCI, 37 mg, 0.192 mmol) and then *N*-hydroxysuccinimide (22 mg, 0.192 mmol). The reaction was stirred for 8 h at rtand then concentrated. The crude was dissolved in 30 mL chloroform and washed with water (3 × 20 mL). The organic layer was concentrated and 30 mL of ethyl ether was added, after which the resulting white precipitate was filtered and redissolved in chloroform (15 mL). This solution was filtered and the filtrate was concentrated to yield the crude NHS ester of **9b** as a colorless oil. The crude NHS ester was then stirred in 1 mL of *N,N*-dimethylformamide, to which was added **4b** (10 mg, 0.0167 mmol) in 1 mL tetraethylammonium bicarbonate (TEAB, 1 M, pH=7.5). Additionally 1 mL of tetrahydrofuran was added to enhance solubility. The reaction was then allowed to stir at rt overnight. The solvent was then removed under reduced pressure, and the solid crude product was washed with acetone (3 × 20 mL). This crude was then dissolved in deionized water to stir with 500 mg of Chelex 100, sodium form at rt for 2 h. The reaction solution was then loaded directly onto a C18 reversed-phase column (2 g) and the column was eluted with deionized water (20 mL). The water elution was lyophilized to yield **2** as a white solid (11 mg, 61%).

^{1}H NMR (300MHz, D_2O) δ 7.71-7.52 (m, 7H), 7.37 (t, *J* = 6 Hz, 2 H), 4.24-4.18 (m, 3H), 3.88-3.63 (m, 10H), 3.03-2.97 (m, 4H), 2.79 (t, *J* = 6 Hz, 2H), 2.10-2.05 (t, *J* = 6Hz, 2H), 1.67-1.68 (m, 1 H), 1.46-1.34 (m, 10H), 1.22-1.16 (m, 9H). ^{31}P NMR (121.5 MHz, D_2O): 1.33, 1.02, 0.40, −0.89. MALDI-HRMS $[M+Na]^+$ calcd for 1095.2178; found 1095.2285

Benzophenone-Lys(alkyne)-hexyl-PI(3,4,5)P_3 (3): Compound **9a** (80 mg, 0.129 mmol) was dissolved in 2 mL of methanol. To this solution was added 2 mL of 2M sodium hydroxide aqueous solution. The reaction was stirred at rt overnight and was then added to proton resin to adjust the pH to ~4, removal of the resin by filtration. The filtrate was next concentrated to yield crude acid **9b** as a colorless gum (68 mg, 87%). Acid **9b** (68 mg, 0.112 mmol) was next dissolved in 6 mL of tetrahydrofuran. To this stirred solution was added *N*-(3-Dimethylaminopropyl)-*N*′-ethylcarbodiimide hydrochloride (EDCI, 43 mg, 0.224 mmol) and then *N*-hydroxysuccinimide (26 mg, 0.224 mmol), and the reaction was stirred for 8 h and then concentrated. The crude was next dissolved in 30 mL of chloroform and washed with water (3 × 20 mL). The organic layer was concentrated and 30 mL of ethyl ether was

added, after which the resulting white precipitate was filtered and redissolved in chloroform (15 mL). The solution was then filtered and the filtrate was concentrated to yield the crude NHS ester corresponding to **9b** as a colorless oil. The crude NHS ester was then dissolved in 1 mL of *N*,*N*-dimethylformamide. To this solution was added **4b**[36] (8 mg, 0.0106 mmol) in 1 mL tetraethylammonium bicarbonate (TEAB, 1 M, pH=7.5). Additionally, 1 mL of tetrahydrofuran was added to enhance solubility. The reaction was next allowed to stir at rt overnight, at which point the solvent was removed under reduced pressure. The solid crude product was washed with acetone (3 × 20 mL) and then dissolved in deionized water to stir with 500 mg of Chelex 100, sodium form at rt for 2 h. The reaction solution was directly loaded onto a C18 reversed-phase column (2 g) and the column was eluted with deionized water (20 mL). The water elution was lyophilized to yield **3** as a white solid (11.2 mg, 93%).

^{1}H NMR (500MHz, D_2O) δ 7.86-7.80 (m, 4H), 7.76-7.74 (m, 2H), 7.67 (t, J = 3 Hz, 1H), 7.53-7.50 (m, 2H), 4.36-4.33 (m, 3H), 4.03-4.02 (m, 1H), 3.96-3.95 (m, 2H), 3.83-3.79 (m, 3H), 3.16-3.02 (m, 5H), 3.02-2.78 (m, 2H), 2.35-2.31 (m, 4H), 2.09-2.06 (m, 2H), 1.80-1.78 (m, 2H), 1.51-1.18 (m, 18H). ^{31}P NMR (202.5 MHz, D_2O): 0.70, 0.31, −0.28, − 0.90. MALDI-HRMS $[M + Na]^+$ calcd for 1208.3024; found 1208.2186.

2. Protein and cell extract labeling studies

General procedure for protein labeling: In a transparent 96-well plate, Akt-PH (50 uL, 60 ug/mL in PBS) or cytosolic cell extracts (50 uL used in samples for probe **1**, 43 uL used in samples for probe **2** and **3,** 1.0 mg/mL in PBS buffer pH 7.4) were incubated with PIP_n probes **1**, **2** or **3** (50× stock in water) or bifunctional tag **8a** (50× stock in DMSO) for 1 h at rt. The 96-well plate was then placed on ice and photolyzed for 1 h by placing it ~ 1 cm below a 365 nm Spectroline ENF260C UV lamp. Samples using probe **2** or **3** were followed by derivatization via click chemistry while samples of probe **1** were directly subjected to SDS-PAGE.

Procedure for click reaction using azido-rhodamine 11 (probe 2 and 3 only).[37,42]: Following the photolysis procedure, to each sample was added 50 uM rhodamine-N_3 **(11)** (50× solution in DMSO), 1mM *tris*(2-carboxyethyl)phosphine (TCEP, 50× solution in water), 100 uM ligand (TBTA or THPTA (**18**), 17× stock in DMSO/*t*-butanol v/v 1:4) and 1 mM Copper sulfate pentahydrate (50× stock in water). Samples were shaken for 10 sec after each addition. After all additions, samples were incubated at rt for 1 hour. For gel analysis, each sample was quenched by adding 50 uL of SDS-PAGE sample buffer (2×). The proteins (30 uL of quenched sample per gel lane) were separated by 1D SDS-PAGE and visualized via in-gel using a fluorescence scanner.

Procedure for competition studies with Akt-PH: Akt-PH protein in PBS buffer pH 7.4 (60 ug/mL) was added into four separate wells of a 96-well microplate (50 uL each). Sample were then incubated with either 0 mM, 2 mM, 5 mM or 10 mM amino-tagged PI(3,4,5)P_3 (**4b**) (50× stock in water) at 4 °C overnight, prior to incubation with 50 uM probe **2** (2.5 mM stock in water) for 1 h. The 96-well plate was then placed on ice and photolyzed for 1 h under 365 nm UV lamp. Next, the click reaction procedure with azido-rhodamine was **11** performed with each sample, followed by SDS-PAGE and fluorescence scanning.

3. Mass Spectrometry Proteomic Analysis

Procedure for sample preparation: To three separate tubes was added cytosolic MDA-MB-435 cancer cell extract (870 μL each, 1 mg/mL in PBS for sample I and II, or 2 mg/mL in PBS for sample III) as well as 20 uL of alkyne−PI(3,4,5)P_3 probe **2** (5 mM stock solution in water for a final concentration of 100 uM in sample I and II or 1.25 mM stock solution in water for a final concentration of 25 uM in sample III). Finally, for sample I and II, a control

sample was generated using the same conditions, but using bifunctional tag **8a** lacking PIP headgroups; for sample III, a control sample was generated using the same condition but lacking the addition of any probe. These samples were incubated for 1 h, followed by photolysis on ice via 350 nm irradiation for 1 hour. Next, 6 uL of biotin-azide **12** (50 mM in DMSO for a final concentration of 300 uM) was added, followed by 20 uL tris-(2-carboxyethyl)phosphine (TCEP, 50 mM in water for a final concentration of 1 mM), 66 uL of TBTA ligand (1.67 mM in 1:4 DMSO/*t*-butanol for a final concentration of 100uM) and 20 uL of copper sulfate pentahydrate (50 mM in water a final concentration of 1 mM). These mixtures were incubated at room temperature for 1 hour. Next, to each sample was added 4 mL of methanol, 1 mL of chloroform and 3 mL of water, and the samples were vortexed and then centrifuged (4,000 rpm for 10 minutes) to pellet proteins. The protein pellet was re-dissolved in 600 uL of methanol, and 150 uL of chloroform along with 600 uL of water were added, after which the samples were vortexed and centrifuged (14,000 rpm for 3 minutes) to pellet the proteins a second time. The protein pellet was then washed with methanol (2 × 600 uL), followed by re-suspension in 500 uL of 6 M urea / 25 mM ammonium bicarbonate. Water (500 uL) was added to each sample, which was then heated to 65 °C for 5 minutes. After addition of 50 uL of TCEP (0.1 M for a final concentration of 10 mM), the sample incubation was continued at 65 °C for 15 min. After the samples were cooled to room temperature, 40 uL of iodoacetamide (0.55 M in 50 mM ammonium bicarbonate for a final concentration of 40 mM iodoacetamide) was added to each sample and the resulting solutions were incubated at 37 °C for 30 min in the dark. Next, 10% SDS was added to achieve a 2% final concentration. The samples were next heated to 65 °C for 5 min and then diluted into 0.2% SDS solution with PBS and 50 mM Tris buffer (v/v 3:3.5). The slurry was then washed with PBS (2×). To this slurry was added strepavidin agarose resin (Thermo Scientific) and the resulting samples were incubated at room temperature for 1 hour with rotation. The resin was centrifuged to pellet (4000 rpm for 3 min) and washed with 1% SDS buffer (2 × 8 mL), 6 M urea (2 × 8 ml) and then PBS buffer (2 × 10 mL). Next, to the resin was resuspended 200 uL of 2 M urea / 25 mM ammonium bicarbonate, 2 uL calcium chloride (100 mM in water for a final concentration of 1 mM) and 4 ug trypsin (sequence grade, Promega). Samples were incubated at 37°C overnight, and were then centrifuged to separate the resin from the supernatant. The supernatant was collected and acidified using 5% formic acid for LC/MS/MS analysis. The data generated from samples containing probe were compared with those from the control studies.

Mass Spectrometry and Data analysis: Digested peptide mixtures were pressure-loaded onto a biphasic (strong cation exchange/reverse phase) capillary column and analyzed by two-dimensional liquid chromatography (2D-LC) separation in combination with tandem mass spectrometry, as has previously been described.[43–45] Mass spectrometry was performed using an Agilent 1200-series quaternary pump and Thermo Scientific LTQ ion trap mass spectrometer. Peptides were eluted in a 5-step MudPIT experiment (using 0%, 10%, 25%, 80%, and 100% salt bumps of 500 mM aqueous ammonium acetate) and data were collected in data-dependent acquisition mode with dynamic exclusion turned on (90 s, repeat of 1). Specifically, one full MS (MS1) scan (400–1800 m/z) was followed by 7 MS_2 scans of the most abundant ions. The MS_2 spectra data were extracted from the raw files using RAW Xtractor (version 1.9.1; publicly available at http://fields.scripps.edu/?q=content/download). MS_2 spectra data were searched using the SEQUEST algorithm (Version 3.0) against the latest version of the mouse IPI database concatenated with the reversed database for assessment of false-discovery rates. In total the search database contained 553 protein sequence entries (549 real sequences and 4 decoy sequences). SEQUEST searches allowed for variable oxidation of methionine (+16.0), static modification of cysteine residues (+57.0 due to alkylation), no enzyme specificity and a mass tolerance set to ±1.5 Da for precursor mass and ±0.5 Da for product ion masses. The

resulting MS2 spectra matches were assembled and filtered using DTASelect (version 2.0.47). The validity of peptide/spectrum matches was assessed using DTASelect and two SEQUEST-defined parameters, the cross-correlation score (XCorr), normalized difference in cross-correlation scores (DeltaCN). The search results were grouped by charge state (+1, +2, +3), tryptic status, and modification status (modified and unmodified peptides), resulting in 18 distinct subgroups. In each of these subgroups, the distribution of Xcorr and DeltaCN values for the direct and decoy database hits was obtained, then the direct and decoy subsets were separated by discriminant analysis. Outlier points in the two distributions were discarded. Full separation of the direct and decoy subsets is not generally possible so the discriminant score was set such that a false discovery rate of less than 0.73 % was determined based on the number of accepted decoy database peptides. In addition, a minimum peptide length of seven amino acids residues was imposed and protein identification required the matching of at least two peptides per protein. Such criteria resulted in the elimination of most decoy database hits. Lists of prospective PI(3,4,5)P_3-binding proteins were generated by setting criteria as ≥ 5-fold (Table 1) or ≥ 2-fold (Table 2) higher spectral counts in samples containing probe **2** compared to the corresponding negative control sample. Three protein lists were generated from separate runs, and all proteins listed in Table 1 or 2 were detected in at least two of the three runs. Protein functions and domains were determined by searching two databases (www.uniprot.org/uniprot, http://pir.georgetown.edu).

Results

Design and synthesis of PIP_n headgroup activity-based probes

Activity-based probes generally consist of analogs of the natural substrate/ligand of interest in which two groups are introduced: 1) a reactive functional group that allows for the covalent labeling of target proteins; and 2) a secondary tag that enables selective detection and/or purification of proteins that have been successfully labeled by the probe. Activity probes corresponding to ligands that interact with proteins solely through non-covalent binding interactions typically employ photoaffinity tags[46] to enforce covalent labeling of target proteins.[33,34,47–49] For this purpose, we implemented the benzophenone group due to its robust nature and ease of synthesis. Based on these principles, our designs for activity probes (**1**–**3**) based on PIP_n headgroups are shown in Figure 1.

The probes illustrated in Figure 1 contain different secondary tags including a fluorescein moiety (**1**) for direct in-gel detection of probe-labeled products or alkynes (**2**,**3**) as latent bioorthogonal[50,51] reactive groups. The alkynes in the latter probes were employed for selective derivatization after protein labeling via click chemistry to introduce rhodamine for in-gel detection or biotin for affinity purification. This approach has proven successful for avoiding disadvantages that can result from initial attachment of bulky reporter tags.[42] In order to introduce the two tags into each structure, we exploited lysine as a Y-shaped linker, with the benzophenone introduced at the α-amino group and the secondary tag appended onto the side chain. Probe **3** included a longer linker between the PIP_n headgroup and the photoaffinity tag since it is known that this distance affects the magnitude of protein cross-linking. Finally, probes corresponding to both PI(3,4)P_2 (**1**) and PI(3,4,5)P_3 (**2**,**3**) were developed and studied.

In structures **1**–**3**, the ligand motif consists of the PIP_n headgroup linked via the traditional phosphodiester at the 1-position to a shortened hexyl linker attached to the reporter groups. Here, the glycerolipid backbone of the PIP_ns is excluded so as to present the photoaffinity tag in closer proximity to bound protein targets to promote labeling. Indeed, close proximity of the benzophenone was found to be important for successful protein labeling (see discussion below). While the short hexyl chain provides hydrophobic character to mimic the

glycerolipid backbone, these simplified headgroup compounds benefit from water solubility. This circumvents the potential concern that the photoaffinity tag may be buried in the membrane core if full phospholipid analogs were used. In addition, hydrophilic probes were expected to be beneficial for avoiding nonspecific protein binding that often results from hydrophobic interactions. Finally, it is known that many proteins bind simplified soluble PIP_n headgroups with high affinity outside of the membrane environment,[52–56] which is particularly the case with heavily phosphorylated isomers such as $PI(3,4,5)P_3$. For each of these reasons, we elected to utilize simplified headgroup probes bearing short hydrophobic moieties.

The synthesis of the described activity probes benefited from significant advances in PIP_n synthetic strategies in recent years.[57–59] We exploited the strategy of using amino-conjugates [60–68] of PIP_n headgroups as modular intermediates that can be efficiently derivatized to produce a range of probes through amide bond formation. For this purpose, we recently described the synthesis of aminohexyl headgroup analogs of type **4** (Scheme 1) corresponding to all seven naturally occurring PIP_n isomers.[36] Using this strategy, probes **1–3** were each synthesized in one step from the appropriate PIP_n headgroup-amino-conjugate, either **4a** to produce $PI(3,4)P_2$ probe **1** or **4b** to generate $PI(3,4,5)P_3$ probes **2** and **3**.

The synthetic routes employed to access the bifunctional lysine handles corresponding to each probe are depicted in Scheme 2. Each of these began with the removal of the carboxybenzyl group (Cbz) of fully protected lysine derivative **5**, followed by coupling of the resulting amino group with benzoylbenzoic acid to introduce the benzophenone photoaffinity tag,[69] and finally Boc deprotection to common intermediate **6**. To produce $PI(3,4)P_2$ probe **1**, compound **6** was coupled to 5(6)-carboxy fluorescein to generate **7a**, followed by ester hydrolysis to carboxylic acid **7b**, which was then converted to the corresponding *N*-hydroxysuccinimidyl (NHS) ester, and finally coupled with amine **4a**. Compounds **2** and **3** were both produced from carboxylic acid **8b**, which was generated through coupling of amine **6** to alkynyl-carboxylic acid **10** to **8a,** followed by ester hydrolysis. Compound **8b** was converted to an NHS ester and coupled to amine **4b** to produce $PI(3,4,5)P_3$ probe **2**. Finally, probe **3** was accessed by coupling **8b** with 6-aminocaproic acid to yield **9a**, followed by ester hydrolysis to **9b**, and conversion to the corresponding NHS ester, which was then coupled with $PI(3,4,5)P_3$ headgroup-amine conjugate **4b**.

Analysis of protein labeling by PIP_n activity probes using the PH domain of Akt as a purified protein target

In order to obtain an initial assessment of the efficacy of the described activity probes for covalently labeling cognate protein binding partners, we performed studies employing the PH domain of Akt as a known target for both $PI(3,4)P_2$ and $PI(3,4,5)P_3$ (Figure 2).[39,70,71] These initial studies were performed by labeling Akt-PH with probes **1** (lanes 1–3) or **2** (lanes 4–5). Labeling experiments were generally performed as follows: Akt-PH was incubated with probe **1** or **2** for 1 hour at room temperature, followed by irradiation on ice with 365 nm light for 1 hour. Experiments involving probe **1** were then directly subjected to 1D SDS-PAGE for on-gel fluorescence analysis due to the presence of fluorescein in the probe. Samples involving probe **2** utilized an intermediate step after photolysis in which click chemistry was exploited to label the alkyne of this probe through reaction with rhodamine-azide **11**, followed by on-gel detection via fluorescence imaging (see section 4 for further details on post-labeling). The results of these experiments showed that Akt-PH was successfully labeled by both $PI(3,4)P_2$−fluorescein probe **1** (Lane 2) and $PI(3,4,5)P_3$−alkyne probe **2** (Lane 4). Please note that a color version of the fluorescence gel image in Figure 1 is also included as Figure S1 in the supplementary information.

A potential concern in any cross-linking experiment is that labeling may result from non-specific interactions of the probe with proteins that are not cognate binding partners. This is particularly the case with photoaffinity tags, which generate highly reactive intermediates upon photolysis. As such, control experiments are important for demonstrating whether labeling events are driven by specific binding interactions. One control study we performed to further scrutinize binding involved the initial heat denaturation of the protein target prior to probe incubation, which should abrogate labeling due to the loss of the protein binding domain upon destruction of its higher order structure. As seen in Figure 2, for both probe **1** (lane 3) and probe **2** (lane 5), initial heat denaturation of Akt-PH negated protein labeling, as was expected. Probe **1** was subjected to an additional control in which irradiation was not performed (lane 1), which also led to no protein labeling. These results demonstrate that the labeling of Akt-PH involves specific binding and that the photoaffinity tag is critical for on-gel detection of protein labeling.

Further control studies designed to verify that the PIP_n headgroup is responsible for protein labeling involved competition binding using soluble unlabeled $PI(3,4,5)P_3$ headgroup analog **4b** and probe **2**. As shown in Figure 3, competition was observed with 40 times excess of inhibitor **4b** and increased with larger concentrations of this competitor up to 200 times excess, which abrogated most of the labeling event (lanes 1–4). Once again, Coomassie Blue stains showed that the protein was still present in each lane (not shown). It is likely that high competitor concentrations are required since probe **2** has a competitive advantage in that it yields irreversible covalent protein labeling, while competitor **4b** acts through reversible non-covalent binding. Finally, to rule out the possibility that the bifunctional lysine tag can label protein on its own, compound **8a** lacking a PIP_n headgroup was also tested for protein labeling (lane 5). Following incubation, cross-linking, and click chemistry with the rhodamine reporter tag, the result showed no labeling of Akt-PH, although it appears that a small impurity in the protein sample just below Akt-PH is labeled in this case. It is possible that **8a** might lead to enhanced non-specific labeling due to the hydrophobicity of this compound, leading it to insert into hydrophobic pockets on random proteins. Indeed, it is plausible that probes **1** and **2** would avoid non-specific labeling events, as was observed through the control studies described herein, due to their hydrophilic nature.

It has previously been observed that the nature of the linker between the ligand motif and a photoaffinity tag can affect the efficiency of protein labeling, in some cases leading to dramatic variations.[47,48,72] In particular, differences in linker lengths can cause noticeable discrepancies in protein labeling. To explore how linker length affected the current studies, we compared probes **2** and **3**, the latter containing a longer linker, in terms of the labeling of Akt-PH (Figure 4). Here, we found that probe **3** exhibited virtually no labeling of Akt-PH (lane 2) when compared to probe **2**. Once again, Coomassie Blue stains showed that the protein remains present in each lane (not shown). These results can be rationalized as follows: while the longer linker provides more flexibility for the bifunctional lysine motif, the benzophenone photoaffinity group can only react with proteins in close proximity, and this flexibility may provide too much freedom such that the benzophenone does not spend enough time proximal to the bound protein. These studies again show that the linker between the ligand moiety and photoaffinity tag is critical for effective protein labeling.

Labeling of proteins in cell extracts using PIP_n probes

Following initial studies involving the labeling of purified Akt-PH protein, we moved on to more complex studies employing cell extracts. The strategy underlying these experiments is depicted in Figure 5, and probe **2** was generally used for studies since click chemistry allows for post-labeling with different reporter groups and this compound was more effective in protein labeling than probe **3**. First, cell lysates were incubated with the probe to allow for

binding of cognate protein binding partners via non-covalent interactions. Next, irradiation with 360 nm light was performed to capture these binding events through covalent cross-linking between the probe and bound proteins. The appropriate tag (rhodamine for in-gel visualization or biotin for affinity purification) was then appended to the protein-probe adducts via click chemistry. We specifically chose cancer cell extracts for studies due to the involvement of PIP_n signaling in tumorigenesis.

Cell extract labeling experiments began by studying a soluble proteome preparation of the human melanoma cell line MDA-MB-435 using various concentrations of probe and azido-rhodamine **11** Experiments were conducted following the protocol outlined in Figure 5 with heat-denatured proteome samples used as controls. The resulting gel showed that a number of fluorescence-labeled protein bands were present (Figure 6). In the heat-denatured controls, certain bands were found to show diminished labeling, particularly in the low mass range. It is also worthwhile to mention that some of the bands were enriched in heat-denatured samples, particularly in the higher mass range. However, it is often difficult to judge whether these enriched proteins were the same ones that were labeled in the regular sample. Images of coomassie blue stained gels showed identical bands for all lanes (now shown), indicating the presence of the same amount of proteins in each sample. From these results, probe concentrations of 25 or 50 micromolar were selected for each of the following labeling studies to optimize the balance between high-intensity labeling and low-intensity background. Please note that a color version of the fluorescence gel image in Figure 6 is also included as Figure S2 in the supplementary information.

Next, both alkyne-labeled probe **2** and fluorescein-labeled probe **1** were used for labeling studies with human MDA-MB-435 soluble proteome (Figure 7). Here, studies involving fluorescein-labeled probe **1** (lane 1) clearly resulted in higher background labeling in the heat denatured control (lane 2) when compared to studies using alkyne probe **2** (lane 4 versus lane 5 (heat denatured)). It is likely that the enhancement in the labeling of heat denatured samples using probe **1** results from non-specific interactions caused by the presence of fluorescein moiety during the protein labeling event. In the heat denatured control involving probe **2** (lane 5), while a number of bands were observed to be weaker compared to the corresponding normal study (lane 4), some enhanced signals likely attributable to non-specific labeling were again observed in the heat denatured sample. Further controls including the absence of probe **2** (lane 6) and lack of irradiation (lane 8) once again demonstrated that both the probe and photocross-linking steps are necessary for protein labeling and on-gel detection. Finally, we analyzed different conditions for post-labeling via click chemistry during studies. It is known that copper-chelating ligands enhance click chemistry reactions, and two different ligand additives were analyzed herein. As with previously described experiments, lanes 1–8 utilized the ligand TBTA[73] to enhance the click reaction. We compared these results to those with THPTA (compound **18**, supporting information) a ligand with enhanced water solubility[74] (lane 9), and found that the protein labeling results were quite similar using the different ligands. As a result, TBTA was employed in subsequent labeling studies since it is commercially available. Please note that a color version of the fluorescence gel image in Figure 6 is also included as Figure S3 in the supplementary information.

Next, we analyzed multiple cancer cell proteomes (MDA-MB-435, MDA-MB-231, MCF7, and T47D) to test the general applicability of this strategy. Both the soluble and membrane fractions of each of these cell extracts were tested and compared using both alkyne probe **2** as well as fluorescein probe **1**, along with heat denatured proteomes (See fluorescent gel image in Figure S4 of the Supplementary Material). Once again, fluorescein-probe **1** yielded significantly enhanced labeling in heat denatured controls, implicating post-labeling as the more effective approach for analysis. The results also demonstrated that the majority of

protein labeling occurred with the soluble portion of the proteomes, which is consistent with the fact that many PIP_n-binding proteins are soluble peripheral proteins that only interact with the membrane surface upon PIP_nbinding. This result is further influenced by the soluble nature of the probes. Finally, it should be noted that probes **1** ($PI(3,4)P_2$) and **2** ($PI(3,4,5)P_3$) correspond to different PIP_n headgroup isomers, and thus it would be expected that they would label a different but overlapping set of proteins.

Using cell extract studies, we once again addressed the issue of the effect of linker length on protein labeling by comparing probes **2** and **3**. As is seen in Figure 8, the results of these experiments mirrored those of Figure 3 in that probe **3** bearing a longer linker yielded minimal labeling compared to **2**. These results further confirm the importance of linker length in probe design. Additionally, bifunctional lysine analog **8a** lacking a PIP_n headgroup again appeared to label different proteins than probe **2**, which is likely attributable to non-specific binding resulting from the hydrophobicity of this compound.

Proteomic analysis for probe-based characterization of labeled proteins using MDA-MB-435 cancer cell extracts

The initial phases of this research demonstrated that PIP_n activity probes are effective for labeling of protein binding targets. Following these results, we set out to apply these probes for proteomic analysis using MDA-MB-435 cell extracts to characterize protein-binding targets. Due to its effectiveness in prior protein labeling studies alkyne-$PI(3,4,5)P_3$ probe **2** was selected for proteomics experiments, which were performed as described in Figure 5. Cell extracts were incubated with probe **2** and irradiated as described previously, followed by reaction with azido-biotin **12**. Subsequently, biotinylated probe-labeled proteins were separated from unlabeled proteins through strepavidin-based affinity chromatography. Enriched proteins were then digested into peptides using trypsin, and the resulting peptide mixture was analyzed by multidimensional liquid chromatography tandem mass spectrometry (LC/LC-MS/MS) using Multidimensional Protein Identification Technology (MudPIT) technique.[45] Peptide sequences were determined using the SEQUEST algorithm[75] and organized and matched to the parent proteins using DTASelect.[76] Spectral counting, a semi-quantitative measure of relative protein abundance, was used in this study to determine proteins enriched in the probe labeled samples.[43,77,78] Additionally, control studies using lysine linker **8a** lacking PIP_n headgroup or lacking any probe were performed side-by-side with these analyses to determine background enrichments.

From these proteomic experiments, 265 proteins were detected with significantly increased spectral counts in probe-labeled samples compared to controls. In these studies, three probe labeled samples were run, and only those proteins that were observed in at least two of these runs and yielded at least two unique spectral counts are included. In addition, proteins that are known to be endogenously biotinylated, such as methylcrotonoyl-CoA carboxylase, were discounted. The resulting proteins are classified based on the average number of spectral counts relative to controls in Table 1 (≥5 fold above control, 97 proteins) and Table 2 (2–5 fold above controls, 168 proteins). While 2–5 fold enrichments in probe-labeled samples (proteins in Table 2) represent relatively low signals, it should be noted that a number of proteins that have previously been implicated as $PI(3,4,5)P_3$ binders appear in Table 2, as is further discussed below. This provides evidence that 2–5 fold enrichments are sufficient for identifying putative targets. Furthermore, modest enrichments are likely attributable to the low efficiencies commonly observed in photoaffinity labeling events, low expression of certain protein targets, and/or non-specific binding of proteins during streptavidin enrichment.

Of the total of 265 proteins that were oberved, many have been identified as $PI(3,4,5)P_3$-binding proteins in previous reports, including affinity chromatography studies. For

example, 38 proteins were among the PI(3,4,5)P_3 binding proteins identified by Catimel and co-workers,[25] 4 proteins coincide with those detected by Dixon and coworkers, [30] and 2 proteins were also identified by Pasquali and coworkers.[24] Proteins that were previously observed in global proteomics screens are indicated with citations in Tables 1 and 2. In 2002, Krugmann and co-workers identified ARAP3 as a novel PI(3,4,5)P_3 binding receptor,[22] while, in our studies, a protein from the same family, ARAP1, was identified, which was also observed by Dixon and co-workers.[30] Similary, while Dixon and co-workers reported Eukaryotic translation initiation factor 4E, we found Eukaryotic translation initiation factors 3E, 4H, 5A and 6. Furthermore, a number of proteins that were detected contain conserved binding modules that are known to target PIP_ns. These included proteins bearing Calponin Homology (CH) (α-actinin-1 and 4, Filamin-A and B, MARE1, Plectin, IQGA1, β-Spectrin-1), Pleckstrin Homology (PH) (ARAP1, β-Spectrin-1, and SWP70), Septin (Septins 2, 7, and 9), 4.1 Protein Ezrin Radixin Moesin (FERM) (moesin, radixin), Huntington Elongation Factor 3 PR65/A TOR (HEAT) (2AAA, GCN1L), Clathrin (Clathrin heavy chain 1) and Annexin (Annexins A1 and A2) domains. One issue with the current study that may or not be general is that a number of known PI(3,4,5)P_3-binding proteins were not observed. This could result from multiple factors that are detailed in the discussion section below.

In addition to known binding properties and domains, the identified proteins also possess many common functional themes, which are again in general agreement with the conserved roles that have emerged from other PIP_n-binding studies. For example, PI(3,4,5)P_3 has commonly been implicated in the regulation of the actin cytoskeleton, and indeed the current studies yielded at least 12 actin-binding proteins, such as gelsolin, twinfilin-2, β-spectrin, fructose-bisphosphate aldolase A, plectin, radixin, myosins and filamins. Tables 1 and 2 also include at least 55 proteins involved in ATP-binding (21%), 7 proteins involved in GTP-binding (Dynamin-1 like protein, ERF3B, EF1A3, Septins 2, 7 and 9), 9 proteins involved in protein transport (α-coatamer, IF5A1, Exportin-2, Importin-11, RAN, Myosin-Ic, Nucleophosmin, Sequestosome-1, and Transportin-3), 3 proteins involved in cell adhesion (leupaxin, PLAK, LPP), and 3 proteins involved in signal transduction (Filamin-B, Leupaxin, 2ABA). Finally, at least 86 of the labeled proteins participate in protein binding (32%), and many common enzymatic activities were present, including at least 29 hydrolases, 19 transferases, 13 oxidoreductases, 14 kinases, 9 isomerases, and 5 lyases.

Another point of interest involves the dependence of protein labeling results on the particular system that is being analyzed. In this case, the fact that studies were performed using a cancer cell line may lead to certain processes, such as actin skeleton regulation, being particularly represented due to disease-related upregulation. In future studies, we will seek to exploit the ability to use ABPP to identify proteomic variations by comparing profiles of normal cells with those associated with a particular conditions, which has previously been performed for cancer,[37,79–81] malaria[82,83], and obesity[84] cell lines. Finally, proteins detected during the current studies that were not previously known to bind PI(3,4,5)P_3 offer putative new targets for this ligand. As is always the case with global proteomic approaches, further work is necessary to confirm specific binding interactions, but these techniques provide a highly efficient avenue for uncovering prospective targets. Furthermore, certain putative targets exhibit important ramifications for future studies. For example, in the current studies, the labeling of PARK7, associated with Parkinson's disease, opens up interesting possibilities and could be scrutinized further.

Discussion

In this study, we designed, synthesized and applied bifunctional activity-based probes corresponding to PIP_ns to label and identify protein targets of these critical ligands. Probes

consisting of PIP_n headgroup analogs decorated with both a photoaffinity tag for cross-linking to bound proteins and a secondary tag for subsequent analysis were found to be effective for labeling protein targets. In particular, the use of an alkyne secondary tag followed by click chemistry provided a versatile approach for both on-gel fluorescence detection and biotin-based affinity purification that also minimized non-specific protein labeling. The latter problem is likely caused by the bulky reporter groups that are present within the probe structure when click chemistry is not used for post-labeling. Initial studies involving the purified PH domain of Akt yielded effective labeling of this protein that was abrogated using competition binding, heat denaturation, no probe and no light controls, indicating specific labeling resulting from a discrete binding interaction. The study of probes containing different linker lengths between the $PI(3,4,5)P_3$ headgroup and bifunctional tag indicated that a shorter linker (probe **2**) resulted in greatly enhanced protein labeling in this particular case. While this does not necessarily mean that the linker length in this probe is optimal, it does clearly show that the spacing of the photoaffinity group is critical for subsequent protein labeling. In fact, the ideal spacer length would likely vary depending upon the specific 3-dimensional structure of the protein target and the proximity of residues. Nevertheless, there should be a range of distances in which cross-linking is feasible before the distance and flexibility of the photoaffinity tag becomes too great for significant protein labeling.

Following optimization of labeling studies and controls using cancer cell extracts, probe **2** was exploited for proteomic analysis for collective identification of protein targets from these samples, which resulted in the identification 265 proteins. The inclusion of previously known $PI(3,4,5)P_3$-binding targets, proteins bearing conserved PIP_n-binding domains, and many proteins involved in processes associated with PIP_ns provides evidence that this approach is effective for detection of specific protein targets. As a result, the other proteins that were observed represent solid candidate target effectors for further study. It should also be noted that the described probe strategy may also pull down proteins that bind the soluble inositol phosphates (InsPs).[85,86] In this case, probe **2** could also be considered an analog of inositol-(1,3,4,5)-tetrakisphosphate, in which the phosphate at the 1-position has been modified for linkage via a phosphodiester, a linkage strategy has previously been pursued to develop probes corresponding to the InsPs.[60–68] Ultimately, the binding properties of InsPs and PIP_ns are often difficult to differentiate due to their similar structures, and indeed members from each family have been observed to compete for the same protein binding targets.[87–90]

One issue with the current study is that a number of known $PI(3,4,5)P_3$-binding proteins were not observed. This could be due to a number of factors including the nature of the probe structures employed for studies, challenges associated with the cross-linking of sufficient quantities of protein for detection, and the use of cell extracts for experiments. One aspect that will affect the proteins that are observed pertains to the structure of the probe that is employed for protein labeling. Previous work has led to the categorization of PIP_n-binding domains based on binding mode, as some proteins bind predominately to the phosphorylated *myo*-inositol headgroup (S-type proteins), others interact with the interfacial membrane region (I-type proteins), and finally a third binding mode involves substantial penetration of the protein into the hydrophobic membrane core (H-type proteins).[4] Since probe **2** corresponds to a soluble headgroup analog, it would be expected that this compound would be more effective at labeling S-type proteins than H-type proteins. This effect can be seen in the data since proteins bearing domains that primarily target headgroups, such as the S-type ANTH and PH modules, were found, while those requiring membrane penetration, such as the H-type ENTH and PX domains, were not.

As discussed previously, soluble activity probes were expected to be beneficial for protein labeling studies to present the photoaffinity tag proximal to bound proteins and avoid non-specific hydrophobic interactions. While this approach may limit the labeling of proteins that require the membrane environment for binding, it will be challenging to devise a single probe structure that will be effective for labeling the majority of PIP_n-binding proteins due to their diverse binding modes. Instead, multiple probes with different structural features will likely be necessary. The need for different structural probes has already been observed in affinity chromatography studies, where isolated beads and those associated with liposomes were found to pull out different and only mildly overlapping sets of proteins.[25] In future studies, we will pursue different probe structures to understand the effect this has on proteins that are labeled. Since PIP_n-binding proteins exhibit broad variation in binding mode in terms of headgroup/membrane binding, localization, multivalency, and requirements for other ligands, diverse probe strategies will likely be necessary to fully elucidate the complex scope of binding targets.

Successful photolabeling of proteins relies on a number of factors including the amount of protein that is effectively labeled, the efficiency of cross-linking and the placement of the photoaffinity tag in close proximity to residues on the bound protein. Low abundance proteins are challenging to detect, which is compounded by the low cross-linking efficiencies commonly observed with photoaffinity groups. Furthermore, proteins should only be labeled when they are in the form in which ligand binding is activated, and lipid-binding proteins are tightly regulated in both a spatial and temporal manner. In addition, the ideal placement of the photoaffinity tag will likely vary for each protein target depending upon the 3-dimensional arrangement of nearby residues in the binding domain. This represents a more general rationale as to why it is unlikely that a single probe structure would be equally effective for labeling all target proteins. While this approach may not pull out every target, it nevertheless provides an efficient means for identifying a set of putative protein targets from highly complex samples. Finally, studies performed using cell extracts may not be ideal since they do not take place in the native environment inside the cell. A primary benefit of ABPP is that this strategy is amenable to analysis using live cells and organisms. Now that these initial PIP_n activity probes have proven effective for labeling and identifying target proteins, we are currently working on modifying probes and conditions to undertake studies in living samples.

Supplementary Material

Refer to Web version on PubMed Central for supplementary material.

References

1. Best MD, Zhang HL, Prestwich GD. Inositol polyphosphates, diphosphoinositol polyphosphates and phosphatidylinositol polyphosphate lipids: Structure, synthesis, and development of probes for studying biological activity. Nat. Prod. Rep. 2010; 27:1403–1430. [PubMed: 20714465]
2. Conway SJ, Miller GJ. Biology-enabling inositol phosphates, phosphatidylinositol phosphates and derivatives. Nat. Prod. Rep. 2007; 24:687–707. [PubMed: 17653355]
3. Lemmon MA. Membrane recognition by phospholipid-binding domains. Nat. Rev. Mol. Cell Biol. 2008; 9:99–111. [PubMed: 18216767]
4. Cho W, Stahelin RV. Membrane-protein interactions in cell signaling and membrane trafficking. Annu. Rev. Biophys. Biomol. Struct. 2005; 34:119–151. [PubMed: 15869386]
5. Di Paolo G, De Camilli P. Phosphoinositides in cell regulation and membrane dynamics. Nature. 2006; 443:651–657. [PubMed: 17035995]
6. Pendaries C, Tronchere H, Plantavid M, Payrastre B. Phosphoinositide signaling disorders in human diseases. FEBS Lett. 2003; 546:25–31. [PubMed: 12829232]

7. Vicinanza M, D'Angelo G, Di Campli A, De Matteis MA. Phosphoinositides as regulators of membrane trafficking in health and disease. Cell. Mol. Life Sci. 2008; 65:2833–2841. [PubMed: 18726176]
8. Wymann MP, Schneiter R. Lipid signalling in disease. Nat. Rev. Mol. Cell Biol. 2008; 9:162–176. [PubMed: 18216772]
9. Assinder SJ, Dong QH, Kovacevic Z, Richardson DR. The TGF-beta, PI3K/Akt and PTEN pathways: established and proposed biochemical integration in prostate cancer. Biochem. J. 2009; 417:411–421. [PubMed: 19099539]
10. Duronio V. The life of a cell: apoptosis regulation by the PI3K/PKB pathway. Biochem. J. 2008; 415:333–344. [PubMed: 18842113]
11. Engelman JA, Luo J, Cantley LC. The evolution of phosphatidylinositol 3-kinases as regulators of growth and metabolism. Nat. Rev. Genet. 2006; 7:606–619. [PubMed: 16847462]
12. Manning BD, Cantley LC. AKT/PKB signaling: Navigating downstream. Cell. 2007; 129:1261–1274. [PubMed: 17604717]
13. Salmena L, Carracedo A, Pandolfi PP. Tenets of PTEN tumor suppression. Cell. 2008; 133:403–414. [PubMed: 18455982]
14. Yuan TL, Cantley LC. PI3K pathway alterations in cancer: variations on a theme. Oncogene. 2008; 27:5497–5510. [PubMed: 18794884]
15. Stokoe D, Stephens LR, Copeland T, Gaffney PRJ, Reese CB, Painter GF, Holmes AB, McCormick F, Hawkins PT. Dual role of phosphatidylinositol-3,4,5-trisphosphate in the activation of protein kinase B. Science. 1997; 277:567–570. [PubMed: 9228007]
16. Katso R, Okkenhaug K, Ahmadi K, White S, Timms J, Waterfield MD. Cellular function of phosphoinositide 3-kinases: Implications for development, immunity, homeostasis, and cancer. Annu. Rev. Cell Dev. Biol. 2001; 17:615–675. [PubMed: 11687500]
17. Maehama T, Dixon JE. The tumor suppressor, PTEN/MMAC1, dephosphorylates the lipid second messenger, phosphatidylinositol 3,4,5-trisphosphate. J. Biol. Chem. 1998; 273:13375–13378. [PubMed: 9593664]
18. Samuels Y, Wang ZH, Bardelli A, Silliman N, Ptak J, Szabo S, Yan H, Gazdar A, Powell DM, Riggins GJ, Willson JKV, Markowitz S, Kinzler KW, Vogelstein B, Velculescu VE. High frequency of mutations of the PIK3CA gene in human cancers. Science. 2004; 304:554–554. [PubMed: 15016963]
19. Chow LML, Baker SJ. PTEN function in normal and neoplastic growth. Cancer Lett. 2006; 241:184–196. [PubMed: 16412571]
20. Rao VR, Corradetti MN, Chen JA, Peng JR, Yuan JY, Prestwich GD, Brugge JS. Expression cloning of protein targets for 3-phosphorylated phosphoinositides. J. Biol. Chem. 1999; 274:37893–37900. [PubMed: 10608855]
21. Painter GF, Thuring JW, Lim ZY, Holmes AB, Hawkins PT, Stephens LR. Synthesis and biological evaluation of a PtdIns(3,4,5)P-3 affinity matrix. Chem. Commun. 2001:645–646.
22. Krugmann S, Anderson KE, Ridley SH, Risso N, McGregor A, Coadwell J, Davidson K, Eguinoa A, Ellson CD, Lipp P, Manifava M, Ktistakis N, Painter G, Thuring JW, Cooper MA, Lim ZY, Holmes AB, Dove SK, Michell RH, Grewal A, Nazarian A, Erdjument-Bromage H, Tempst P, Stephens LR, Hawkins PT. Identification of ARAP3, a novel PI3K effector regulating both Arf and Rho GTPases, by selective capture on phosphoinositide affinity matrices. Mol. Cell. 2002; 9:95–108. [PubMed: 11804589]
23. Lim ZY, Thuring JW, Holmes AB, Manifava M, Ktistakis NT. Synthesis and biological evaluation of a PtdIns(4,5)P-2 and a phosphatidic acid affinity matrix. J. Chem. Soc. Perkin Trans. 2002; 1:1067–1075.
24. Pasquali C, Bertschy-Meier D, Chabert C, Curchod ML, Arod C, Booth R, Mechtler K, Vilbois F, Xenarios I, Ferguson CG, Prestwich GD, Camps M, Rommel C. A chemical proteomics approach to phosphatidylinositol 3-kinase signaling in macrophages. Mol. Cell. Proteomics. 2007; 6:1829–1841. [PubMed: 17617665]
25. Catimel B, Yin MX, Schieber C, Condron M, Patsiouras H, Catimel J, Robinson D, Wong LSM, Nice EC, Holmes AB, Burgess AW. PI(3,4,5)P3 Interactome. J. Proteome Res. 2009; 8:3712–3726. [PubMed: 19463016]

26. Catimel B, Schleber C, Condron M, Patsiouras H, Connolly L, Catimel J, Nice EC, Burgess AW, Holmes AB. The PI(3,5)P2 and PI(4,5)P2 Interactomes. J. Proteome Res. 2008; 7:5295–5313. [PubMed: 19367725]
27. Conway SJ, Gardiner J, Grove SJA, Johns MK, Lim Z-Y, Painter GF, Robinson DEJE, Schieber C, Thuring JW, Wong LS-M, Yin M-X, Burgess AW, Catimel B, Hawkins PT, Ktistakis NT, Stephens L, Holmes AB. Synthesis and biological investigation of phosphatidylinositol phosphate affinity probes. Org. Biomol. Chem. 2010; 8:66–76. [PubMed: 20024134]
28. Tanaka K, ImajohOhmi S, Sawada T, Shirai R, Hashimoto Y, Iwasaki S, Kaibuchi K, Kanaho Y, Shirai T, Terada Y, Kimura K, Nagata S, Fukui Y. A target of phosphatidylinositol 3,4,5-trisphosphate with a zinc finger motif similar to that of the ADP-ribosylation-factor GTPase-activating protein and two pleckstrin homology domains. Eur. J. Biochem. 1997; 245:512–519. [PubMed: 9151987]
29. Wang DS, Ching TT, St Pyrek J, Chen CS. Biotinylated phosphatidylinositol 3,4,5-trisphosphate as affinity ligand. Anal. Biochem. 2000; 280:301–307. [PubMed: 10790314]
30. Dixon MJ, Gray A, Boisvert FM, Agacan M, Morrice NA, Gourlay R, Leslie NR, Downes CP, Batty IH. A screen for novel phosphoinositide 3-kinase effector proteins. Mol. Cell. Proteomics. 2011; 10 10.1074/mcp.M1110.003178.
31. Zhu H, Bilgin M, Bangham R, Hall D, Casamayor A, Bertone P, Lan N, Jansen R, Bidlingmaier S, Houfek T, Mitchell T, Miller P, Dean RA, Gerstein M, Snyder M. Global analysis of protein activities using proteome chips. Science. 2001; 293:2101–2105. [PubMed: 11474067]
32. Cravatt BF, Wright AT, Kozarich JW. Activity-based protein profiling: From enzyme chemistry. Annu. Rev. Biochem. 2008; 77:383–414. [PubMed: 18366325]
33. Gubbens J, Ruijter E, de Fays LEV, Damen JMA, de Kruijff B, Slijper M, Rijkers DTS, Liskamp RMJ, de Kroon A. Photocrosslinking and click chemistry enable the specific detection of proteins interacting with phospholipids at the membrane interface. Chem. Biol. 2009; 16:3–14. [PubMed: 19171301]
34. Gubbens J, de Kroon A. Proteome-wide detection of phospholipidprotein interactions in mitochondria by photocrosslinking and click chemistry. Mol. Biosyst. 2010; 6:1751–1759. [PubMed: 20544074]
35. Tully SE, Cravatt BF. Activity-based probes that target functional subclasses of phospholipases in proteomes. J. Am. Chem. Soc. 2010; 132:3264–3265. [PubMed: 20178358]
36. Gong D, Bostic HE, Smith MD, Best MD. Synthesis of modular headgroup conjugates corresponding to all seven phosphatidylinositol polyphosphate isomers for convenient probe generation. Eur. JOrg. Chem. 2009:4170–4179.
37. Speers AE, Cravatt BF. Profiling enzyme activities in vivo using click chemistry methods. Chem. Biol. 2004; 11:535–546. [PubMed: 15123248]
38. Hong V, Presolski SI, Ma C, Finn MG. Analysis and Optimization of Copper-Catalyzed Azide-Alkyne Cycloaddition for Bioconjugation. Angew. Chem. Int. Edit. 2009; 48:9879–9883.
39. Manna D, Albanese A, Park WS, Cho W. Mechanistic basis of differential cellular responses of phosphatidylinositol 3,4-bisphosphate- and phosphatidylinositol 3,4,5-trisphosphate-binding pleckstrin homology domains. J. Biol. Chem. 2007; 282:32093–32105. [PubMed: 17823121]
40. Smith MD, Gong DH, Sudhahar CG, Reno JC, Stahelin RV, Best MD. Synthesis and convenient functionalization of azide-labeled diacylglycerol analogues for modular access to biologically active lipid probes. Bioconjugate Chem. 2008; 19:1855–1863.
41. Guichard G, Fournel S, Trouche N, Wieckowski S. Preparation of new multimeric molecules, particularly CD40 ligands, for use in the preparation of drugs. 2008
42. Speers AE, Adam GC, Cravatt BF. Activity-based protein profiling in vivo using a coppeRI)-catalyzed azide-alkyne 3+2 cycloaddition. J. Am. Chem. Soc. 2003; 125:4686–4687. [PubMed: 12696868]
43. Jessani N, Niessen S, Wei BQQ, Nicolau M, Humphrey M, Ji YR, Han WS, Noh DY, Yates JR, Jeffrey SS, Cravatt BF. A streamlined platform for high-content functional proteomics of primary human specimens. Nat. Methods. 2005; 2:691–697. [PubMed: 16118640]

44. Peng JM, Elias JE, Thoreen CC, Licklider LJ, Gygi SP. Evaluation of multidimensional chromatography coupled with tandem mass spectrometry (LC/LCMS/ MS) for large-scale protein analysis: The yeast proteome. J. Proteome Res. 2003; 2:43–50. [PubMed: 12643542]
45. Washburn MP, Wolters D, Yates JR. Large-scale analysis of the yeast proteome by multidimensional protein identification technology. Nat. Biotechnol. 2001; 19:242–247. [PubMed: 11231557]
46. Dorman G, Prestwich GD. Using photolabile ligands in drug discovery and development. Trends Biotechnol. 2000; 18:64–77. [PubMed: 10652511]
47. Ballell L, Alink KJ, Slijper M, Versluis C, Liskamp RMJ, Pieters RJ. A new chemical probe for proteomics of carbohydrate-binding proteins. ChemBioChem. 2005; 6:291–295. [PubMed: 15578642]
48. Ballell L, van Scherpenzeel M, Buchalova K, Liskamp RMJ, Pieters RJ. A new chemical probe for the detection of the cancer-linked galectin-3. Org. Biomol. Chem. 2006; 4:4387–4394. [PubMed: 17102885]
49. van Scherpenzeel M, van der Pot M, Arnusch CJ, Liskamp RMJ, Pieters RJ. Detection of galectin-3 by novel peptidic photoprobes. Bioorg. Med. Chem. Lett. 2007; 17:376–378. [PubMed: 17095228]
50. Sletten EM, Bertozzi CR. Bioorthogonal chemistry: Fishing for selectivity in a sea of functionality. Angew. Chem., Int. Edit. 2009; 48:6974–6998.
51. Best MD. Click chemistry and bioorthogonal reactions: unprecedented selectivity in the labeling of biological molecules. Biochemistry. 2009; 48:6571–6584. [PubMed: 19485420]
52. Ferguson KM, Lemmon MA, Schlessinger J, Sigler PB. Structure of the high-affinity complex of inositol trisphosphate with a phospholipase-C pleckstrin homology domain. Cell. 1995; 83:1037–1046. [PubMed: 8521504]
53. Garcia P, Gupta R, Shah S, Morris AJ, Rudge SA, Scarlata S, Petrova V, McLaughlin S, Rebecchi MJ. The pleckstrin homology domain of phospholipase C-delta(1) binds with high affinity to phosphatidylinositol 4,5- bisphosphate in bilayer membranes. Biochemistry. 1995; 34:16228–16234. [PubMed: 8519781]
54. Hirose K, Kadowaki S, Tanabe M, Takeshima H, Iino M. Spatiotemporal dynamics of inositol 1,4,5-trisphosphate that underlies complex Ca2+ mobilization patterns. Science. 1999; 284:1527–1530. [PubMed: 10348740]
55. Kavran JM, Klein DE, Lee A, Falasca M, Isakoff SJ, Skolnik EY, Lemmon MA. Specificity and promiscuity in phosphoinositide binding by Pleckstrin homology domains. J. Biol. Chem. 1998; 273:30497–30508. [PubMed: 9804818]
56. Lemmon MA, Ferguson KM, Obrien R, Sigler PB, Schlessinger J. Specific and high-affinity binding of inositol phosphates to an isolated pleckstrin homology domain. Proc. Natl. Acad. Sci. U. S. A. 1995; 92:10472–10476. [PubMed: 7479822]
57. Prestwich GD. Touching all the bases: Synthesis of inositol polyphosphate and phosphoinositide affinity probes from glucose. Acc. Chem. Res. 1996; 29:503–513.
58. Gu QM, Prestwich GD. Synthesis of phosphotriester analogues of the phosphoinositides PtdIns(4,5)P-2 and PtdIns(3,4,5)P-3. J. Org. Chem. 1996; 61:8642–8647.
59. Painter GF, Grove SJA, Gilbert IH, Holmes AB, Raithby PR, Hill ML, Hawkins PT, Stephens L. General synthesis of 3-phosphorylated myoinositol phospholipids and derivatives. J. Chem. Soc., Perkin Trans. 1999; 1:923–935.
60. Henne V, Mayr GW, Grabowski B, Koppitz B, Soling HD. Smisynthetic derivatives of inositol 1,4,5-trisphosphate substituted at the 1-phosphate group - Effects on calium release from permeabilized guinea-pig parotid acinar cells and comparison with binding to alolase-A. Eur. J. Biochem. 1988; 174:95–101. [PubMed: 3259506]
61. Dorman G, Chen J, Prestwich GD. Synthesis of D-myo-P-1-(Oaminopropyl)- inositol-1,4,5-trisphosphate affinity probes from alpha d-glucose. Tetrahedron Lett. 1995; 36:8719–8722.
62. Inoue T, Kikuchi K, Hirose K, Iino M, Nagano T. Synthesis and evaluation of 1-position-modified inositol 1,4,5-trisphosphate analogs. Bioorg. Med. Chem. Lett. 1999; 9:1697–1702. [PubMed: 10397504]

63. Marecek JF, Estevez VA, Prestwich GD. New tetherable derivatives of myo-inositol 2,4,5-trisphosphates and 1,3,4-trisphosphates. Carbohyd. Res. 1992; 234:65–73.
64. Nakanishi W, Kikuchi K, Inoue T, Hirose K, Iino M, Nagano T. Hydrophobic modifications at 1-phosphate of inositol 1,4,5-trisphosphate analogues enhance receptor binding. Bioorg. Med. Chem. Lett. 2002; 12:911–913. [PubMed: 11958992]
65. Olszewski JD, Dorman G, Elliott JT, Hong Y, Ahern DG, Prestwich GD. Tethered benzophenone reagents for the synthesis of photoactivatable ligands. Bioconjugate Chem. 1995; 6:395–400.
66. Prestwich GD, Marecek JF, Mourey RJ, Theibert AB, Ferris CD, Danoff SK, Snyder SH. Tethered IP3 - synthesis and biochemical applications of the 1- O-(3-aminopropyl) ester of inositol 1,4,5-trisphosphate. J. Am. Chem. Soc. 1991; 113:1822–1825.
67. Schafer R, Nehlssahabandu M, Grabowsky B, Dehlingerkremer M, Schulz I, Mayr GW. Synthesis and application of photoaffinity analogs of inositol 1,4,5- trisphosphate selectively substituted at the 1-phosphate group. Biochem. J. 1990; 272:817–825. [PubMed: 2176480]
68. Tegge W, Ballou CE. Syntheses of D-myo-Inositol 1,4,5-trisphosphate affinity ligands. Carbohyd. Res. 1992; 230:63–77.
69. Smith MD, Sudhahar CG, Gong D, Stahelin RV, Best MD. Modular synthesis of biologically active phosphatidic acid probes using click chemistry. Mol. Biosyst. 2009:962–972. [PubMed: 19668861]
70. Frech M, Andjelkovic M, Ingley E, Reddy KK, Falck JR, Hemmings BA. High affinity binding of inositol phosphates and phosphoinositides to the Pleckstrin homology domain of RAC protein kinase B and their influence on kinase activity. J. Biol. Chem. 1997; 272:8474–8481. [PubMed: 9079675]
71. James SR, Downes CP, Gigg R, Grove SJA, Holmes AB, Alessi DR. Specific binding of the Akt-1 protein kinase to phosphatidylinositol 3,4,5- trisphosphate without subsequent activation. Biochem. J. 1996; 315:709–713. [PubMed: 8645147]
72. Baker JG, Middleton R, Adams L, May LT, Briddon SJ, Kellam B, Hill SJ. Influence of fluorophore and linker composition on the pharmacology of fluorescent adenosine A(1) receptor ligands. Brit. J. Pharmacol. 2010; 159:772–786. [PubMed: 20105183]
73. Wang Q, Chan TR, Hilgraf R, Fokin VV, Sharpless KB, Finn MG. Bioconjugation by coppeRI)-catalyzed azide-alkyne [3+2] cycloaddition. J. Am. Chem. Soc. 2003; 125:3192–3193. [PubMed: 12630856]
74. Chan TR, Hilgraf R, Sharpless KB, Fokin VV. Polytriazoles as coppeRI)-stabilizing ligands in catalysis. Org. Lett. 2004; 6:2853–2855. [PubMed: 15330631]
75. Yates, Eng JK, McCormack AL, Schieltz D. Method to correlate tandem mass-spectra of modified peptides to amino-acid sequences in the protein database. Anal. Chem. 1995; 67:1426–1436. [PubMed: 7741214]
76. Tabb DL, McDonald WH, Yates JR. DTASelect and contrast: Tools for assembling and comparing protein identifications from shotgun proteomics. J. Proteome Res. 2002; 1:21–26. [PubMed: 12643522]
77. Zybailov B, Coleman MK, Florens L, Washburn MP. Correlation of relative abundance ratios derived from peptide ion chromatograms and spectrum counting for quantitative proteomic analysis using stable isotope labeling. Anal. Chem. 2005; 77:6218–6224. [PubMed: 16194081]
78. Usaite R, Wohlschlegel J, Venable JD, Park SK, Nielsen J, Olsson L, Yates JR. Characterization of global yeast quantitative proteome data generated from the wild-type and glucose repression Saccharomyces cerevisiae strains: The comparison of two quantitative methods. J. Proteome Res. 2008; 7:266–275. [PubMed: 18173223]
79. Chiang KP, Niessen S, Saghatelian A, Cravatt BF. An enzyme that regulates ether lipid signaling pathways in cancer annotated by multidimensional profiling. Chem. Biol. 2006; 13:1041–1050. [PubMed: 17052608]
80. Jessani N, Liu YS, Humphrey M, Cravatt BF. Enzyme activity profiles of the secreted and membrane proteome that depict cancer cell invasiveness. Proc. Natl. Acad. SciU.SA. 2002; 99:10335–10340.
81. Paulick MG, Bogyo M. Application of activity-based probes to the study of enzymes involved in cancer progression. Curr. Opin. Gen. Dev. 2008; 18:97–106.

82. Greenbaum DC, Baruch A, Grainger M, Bozdech Z, Medzihradszky KF, Engel J, DeRisi J, Holder AA, Bogyo M. A role for the protease falcipain 1 in host cell invasion by the human malaria parasite. Science. 2002; 298:2002–2006. [PubMed: 12471262]

83. Arastu-Kapur S, Ponder EL, Fonovic UP, Yeoh S, Yuan F, Fonovic M, Grainger M, Phillips CI, Powers JC, Bogyo M. Identification of proteases that regulate erythrocyte rupture by the malaria parasite Plasmodium falciparum. Nat. Chem. Biol. 2008; 4:203–213. [PubMed: 18246061]

84. Barglow KT, Cravatt BF. Discovering disease-associated enzymes by proteome reactivity profiling. Chem. Biol. 2004; 11:1523–1531. [PubMed: 15556003]

85. Irvine RF. Inositide evolution - towards turtle domination? J. Physiol. 2005; 566:295–300. [PubMed: 15860522]

86. Irvine RF, Schell MJ. Back in the water: The return of the inositol phosphates. Nat. Rev. Mol. Cell Biol. 2001; 2:327–338. [PubMed: 11331907]

87. Razzini G, Berrie CP, Vignati S, Broggini M, Mascetta G, Brancaccio A, Falasca M. Novel functional PI 3-kinase antagonists inhibit cell growth and tumorigenicity in human cancer cell lines. FASEB. J. 2000; 14:1179–1187. [PubMed: 10834940]

88. Piccolo E, Vignati S, Maffucci T, Innominato PF, Riley AM, Potter BVL, Pandolfi PP, Broggini M, Iacobelli S, Innocenti P, Falasca M. Inositol pentakisphosphate promotes apoptosis through the PI3-K/Akt pathway. Oncogene. 2004; 23:1754–1765. [PubMed: 14755253]

89. Riley AM, Guedat P, Schlewer G, Spiess B, Potter BVL. A conformationally restricted cyclic phosphate analogue of inositol trisphosphate: Synthesis and physicochemical properties. J. Org. Chem. 1998; 63:295–305.

90. Maffucci T, Piccolo E, Cumashi A, Iezzi M, Riley AM, Saiardi A, Godage HY, Rossi C, Broggini M, Iacobelli S, Potter BVL, Innocenti P, Falasca M. Inhibition of the phosphatidylinositol 3-kinase/Akt pathway by inositol pentakisphosphate results in antiangiogenic and antitumor effects. Cancer Res. 2005; 65:8339–8349. [PubMed: 16166311]

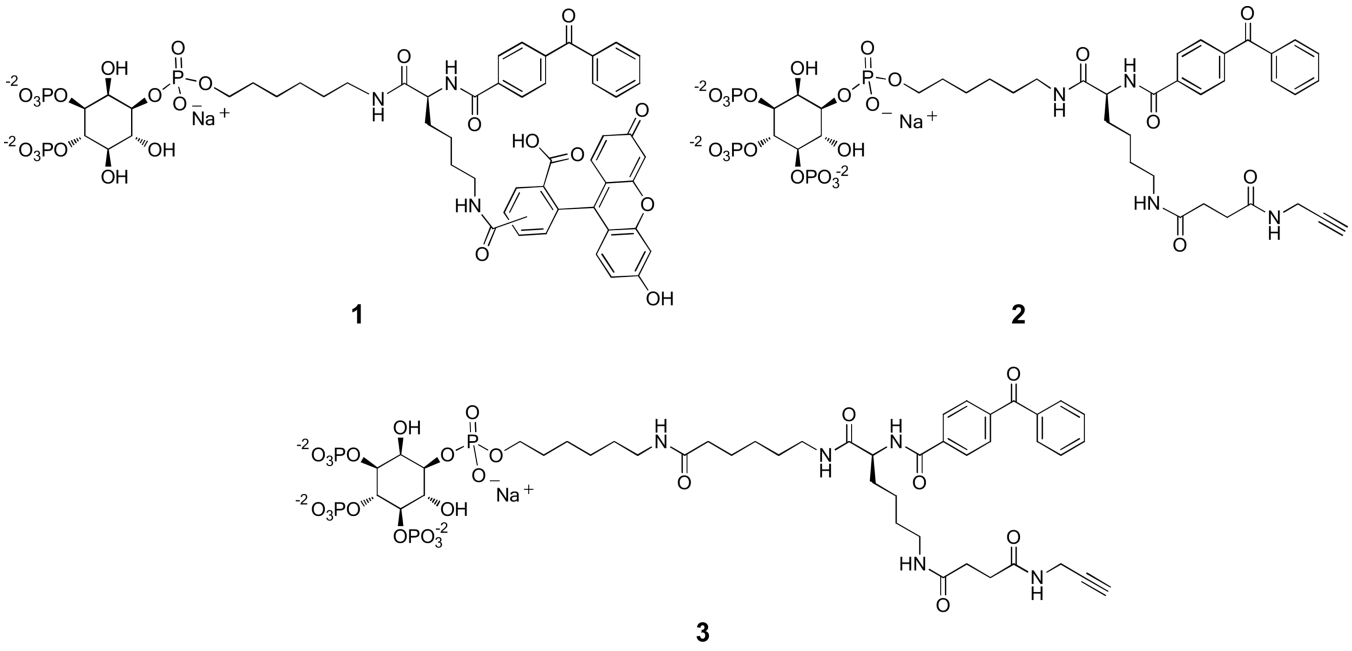

Figure 1.

Design of bifunctional PIPn activity-based probes. Probes consist of the binding moiety (PIPn headgroup), linked to a Y-shaped lysine linker containing both a photoaffinity group (benzophone) and a secondary tag that consisted of either fluorescein (probe **1**) or an alkyne as a bioorthogonal tag (probes **2–3**).

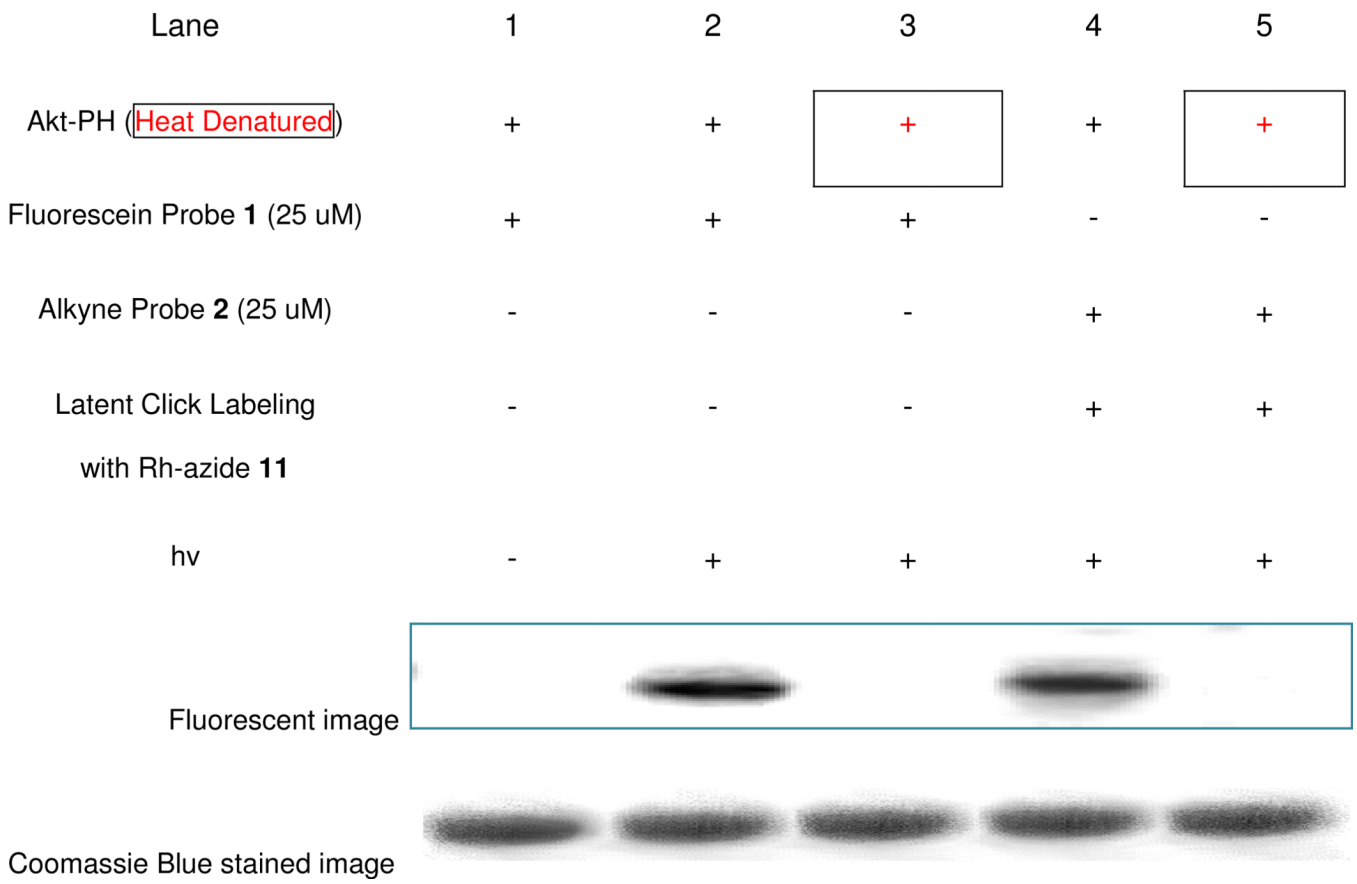

Figure 2.

Gel images of labeling studies using purified Akt-PH (fluorescent gel image shown in grey scale). Studies indicated successful labeling of Akt-PH protein by both fluorescein-probe **1** (lane 2) and alkyne-probe **2** (lane 4, after click chemistry post-derivatization) during studies. Additionally, control studies involving no photo-cross-linking (lane 1), or heat denaturation of the protein prior to probe incubation (lanes 3 and 5) yielded no fluorescence, indicating the absence of non-specific labeling. Finally, Coomassie Blue stains indicate that the protein is still present despite the abrogation of probe labeling. Please also see color fluorescence gel scans in Figure S1 of the supplementary information.

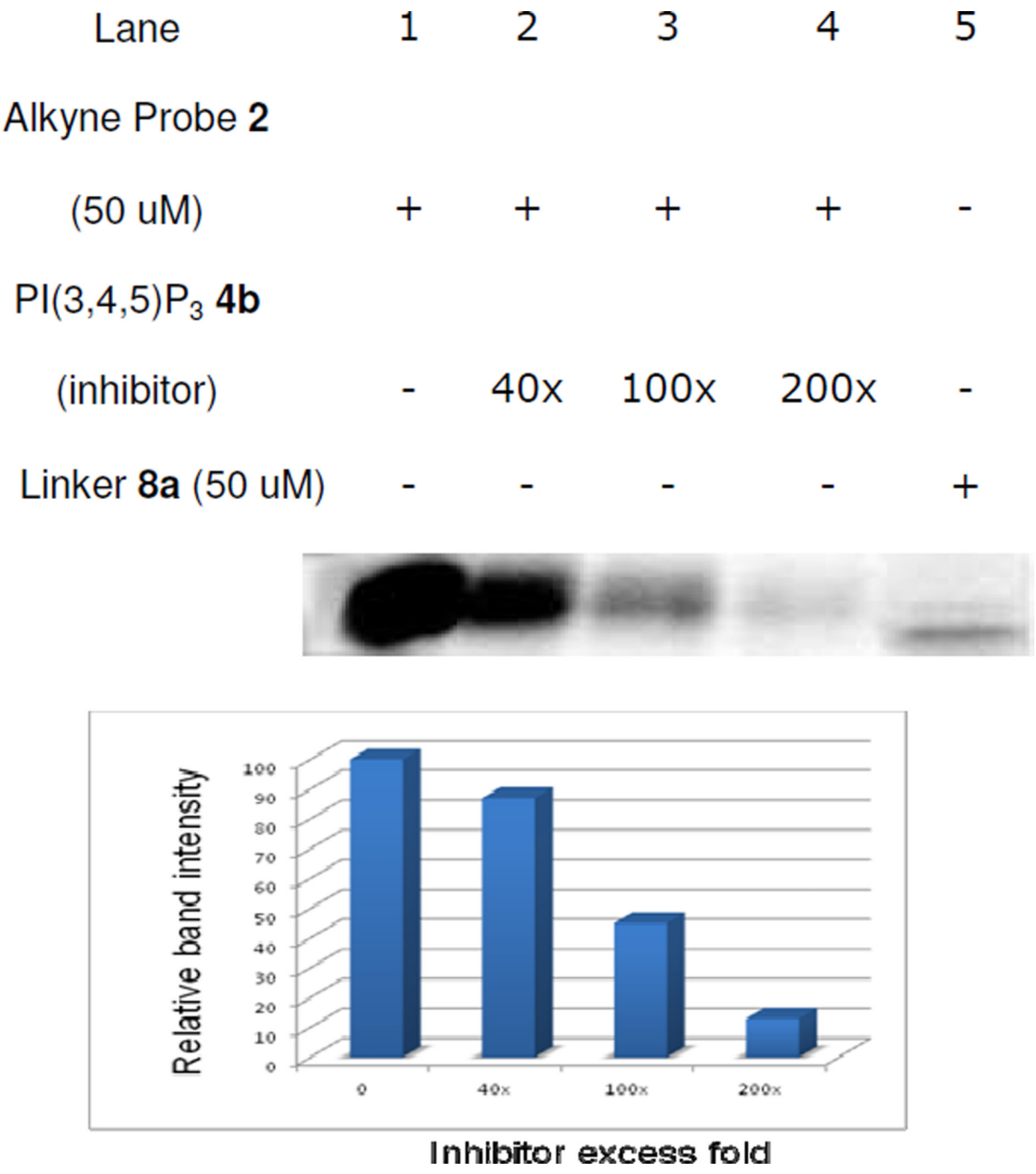

Figure 3.

Competition studies involving Akt-PH labeling (fluorescent gel image shown in grey scale). In lanes 1–4, pre-incubation of Akt-PH with excess inhibitor **4b** suppressed labeling by probe **2** as visualized by a reduction in fluorescence intensity of the AKt-PH band. In lane 5, the bifunctional lysine lacking the PIP headgroup did not label the Akt protein.

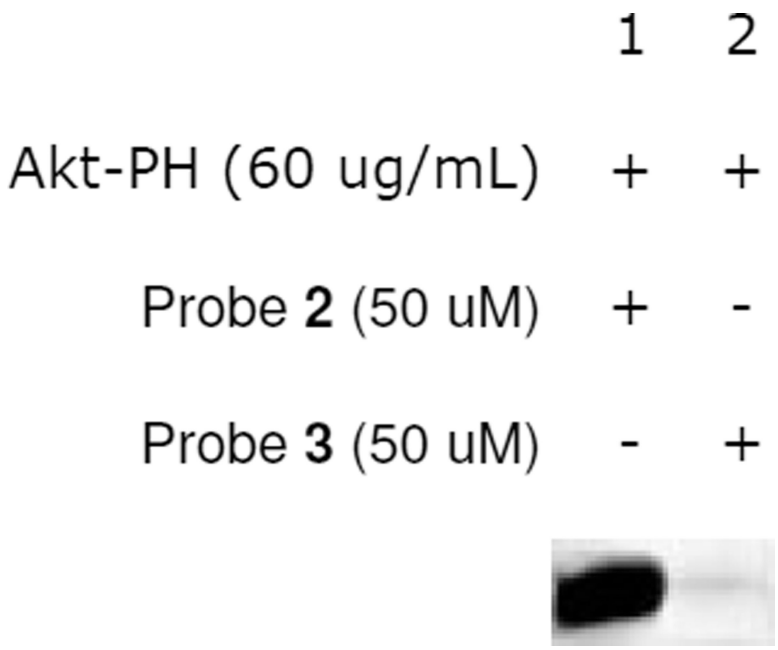

Figure 4.
Akt-PH labeling studies with probes **2** and **3** indicate that the shorter linker (probe **2**) results in significantly enhanced protein labeling (fluorescent gel image shown in grey scale).

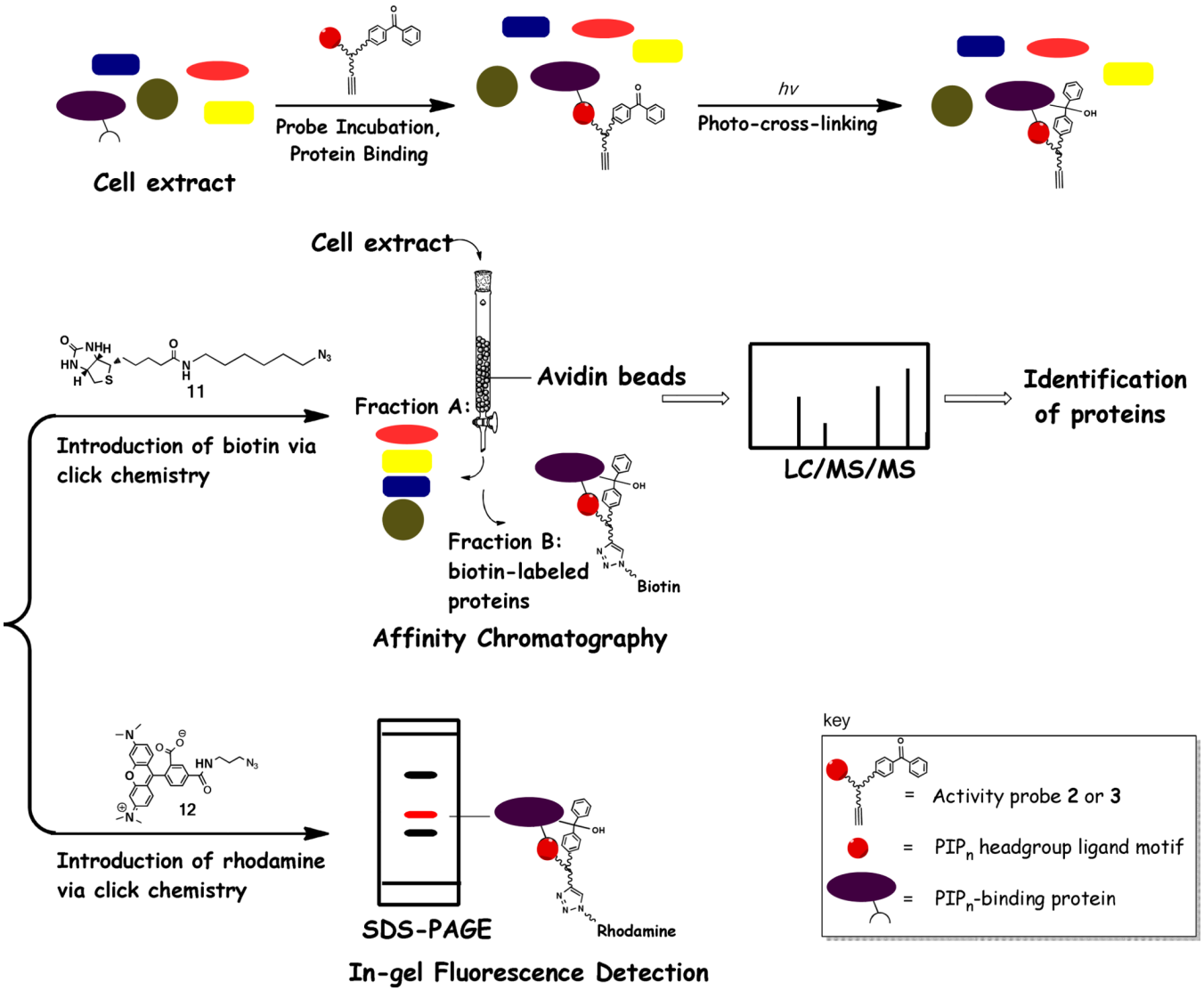

Figure 5.

Illustration of the mechanisms of protein labeling and subsequent analysis using alkynyl-PI(3,4,5)P3 activity probes **2** and **3**. Following the incubation of the probes with cell extracts, protein−probe binding events were captured through irradiation of the benzophenone tag. Next, labeled proteins were selectively derivatized via click chemistry using the secondary functional tag of the probe to introduce rhodamine (**11**) for in-gel fluorescence analysis or biotin (**12**) for protein enrichment via affinity chromatography and subsequent protein identification using liquid chromatography-tandem mass spectrometry.

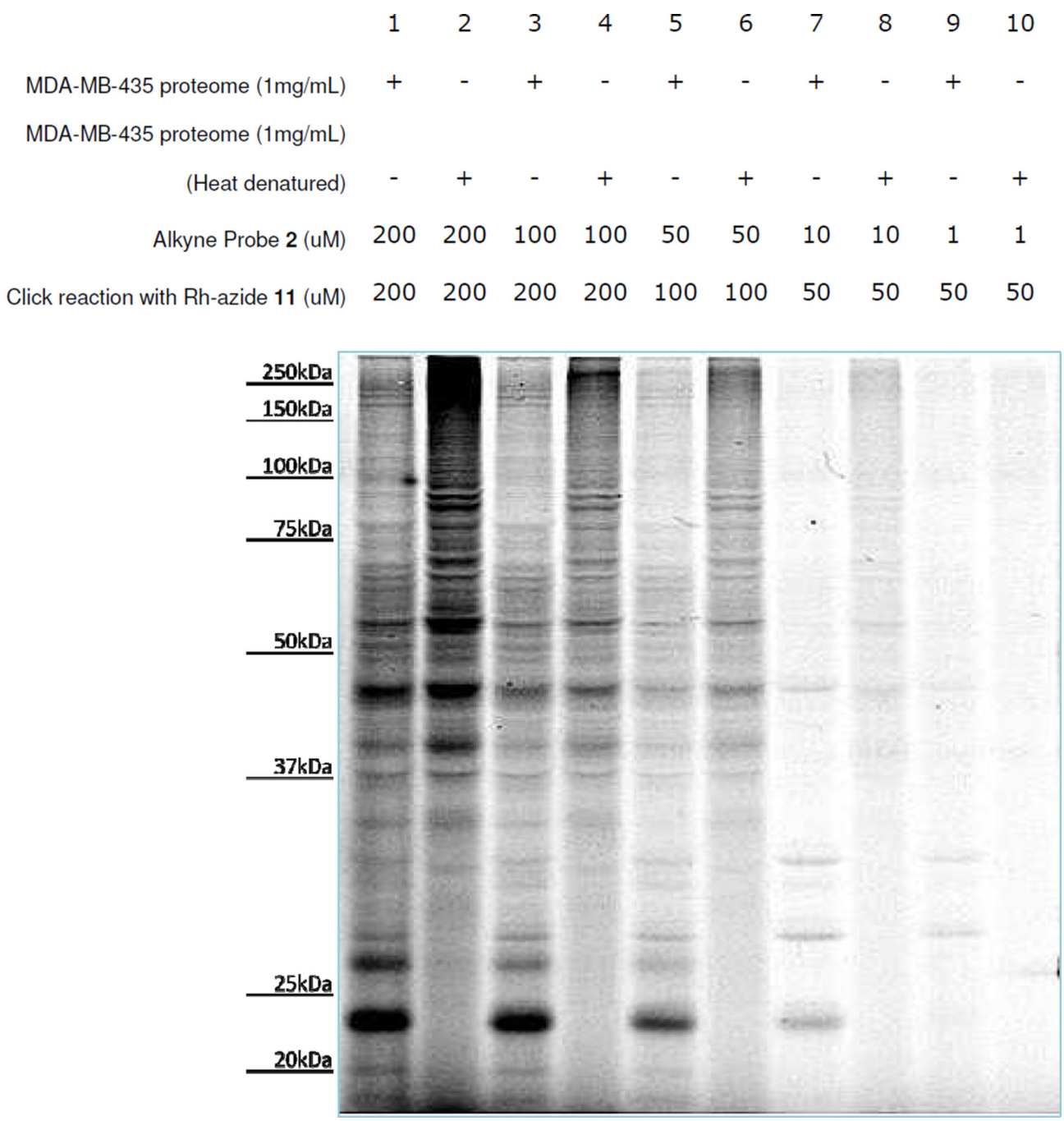

Figure 6.

Labeling studies to ascertain effective probe concentrations (fluorescent gel image shown in grey scale). Probe concentrations were screened using MDA-MB-435 cancer cell extracts (soluble fraction) to identify concentrations that were effective for studies. Concentrations ranging from 200 nM to 1nM were used to label the same amount of the cell extracts with heat-denatured controls performed for each protein concentration. From fluorescence gel imaging results, probe concentrations of approximately 50 μM (lanes 5 and 6) were selected for other labeling studies. Please also see color fluorescence gel scans in Figure S2 of the supplementary information.

	1	2	3	4	5	6	7	8	9
MDA-MB-435 proteome (1mg/mL)	+	-	+	+	-	+	+	+	+
MDA-MB-435 proteome (1mg/mL) (Heat denatured)	-	+	-	-	+	-	-	-	-
Alkyne Probe **2** (25 uM)	-	-	-	+	+	-	+	+	+
Fluorescein Probe **1** (25 uM)	+	+	+	-	-	-	-	-	-
Click rxn with Rh-azide (50uM)	-	-	-	+	+	+	+	+	+
hv	+	+	-	+	+	+	+	-	+
ligand TBTA	+	+	+	+	+	+	+	+	-
ligand THPTA	-	-	-	-	-	-	-	-	+

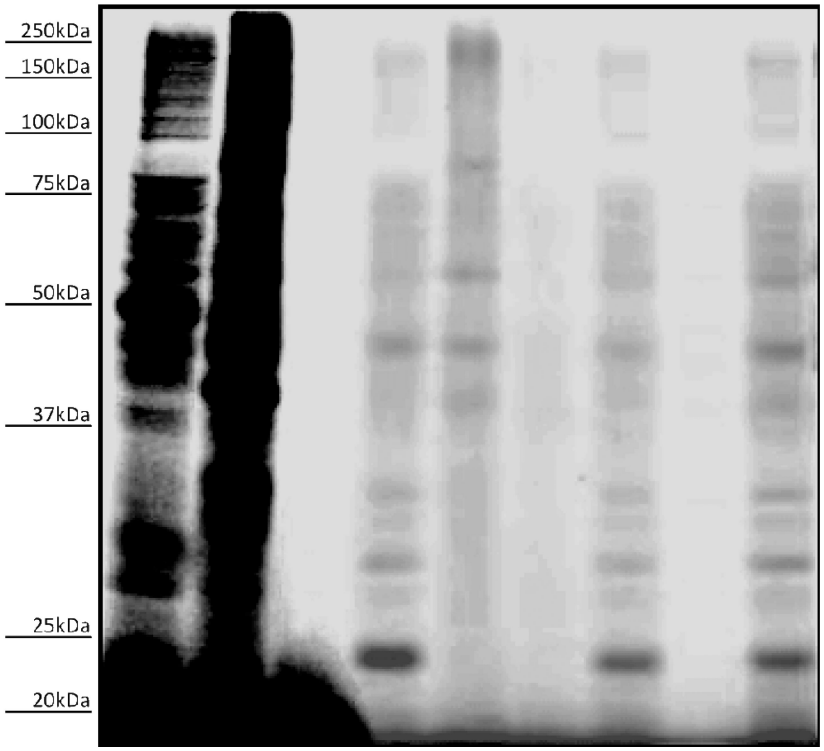

Figure 7.

Labeling of MDA-MB-435 soluble proteome using various conditions (fluorescent gel image shown in grey scale). Studies using fluorescein-probe 1 resulted in significantly stronger labeling in the heat denatured control (lane 2) compared to the normal study (lane 1), indicating that the presence of the fluorophore during labeling is problematic. Studies using probe **2** and post-labeling led to diminished labeling in heat-the denatured control (lane 5, when compared to lane 4). No probe (lane 6) and no light (lane 8) controls negated labeling, and click chemistry ligands TBTA (lane 7) and THPTA (lane 9) yielded similar results. Please also see color fluorescence gel scans in Figure S3 of the supplementary information.

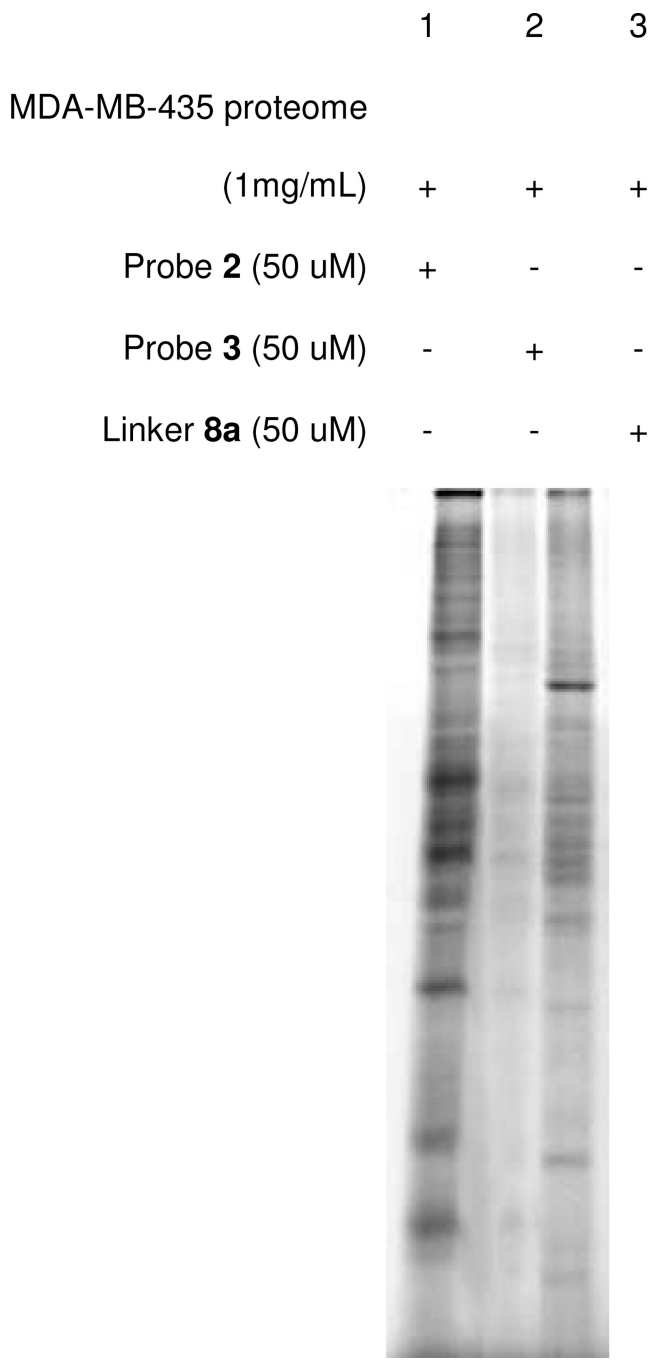

Figure 8.
Analysis of the effect of probe linker length using MDA-MB-435 cancer cell extracts (fluorescent gel image). Labeling studies with probe **2** (shorter linker) yielded significantly enhanced labeling compared to probe **3**. Control compound **8a** lacking the PIPn headgroup yielded minimal protein labeling of an orthogonal subset of proteins.

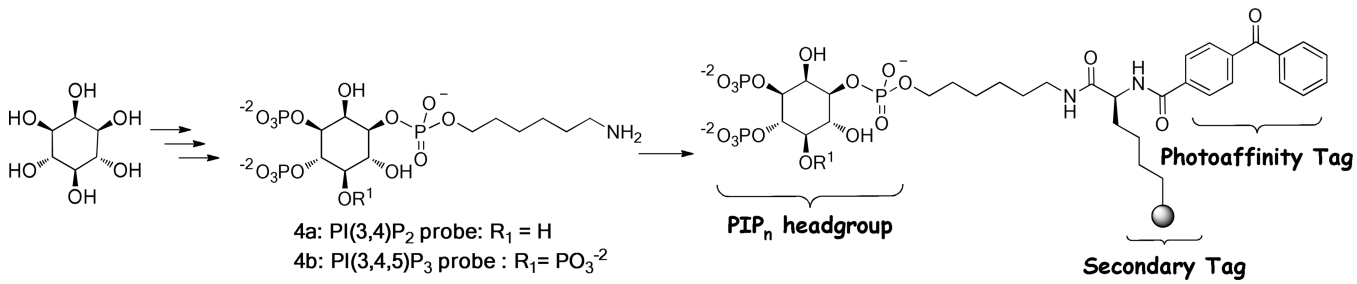

Scheme 1.
General synthetic route to PIPn activity probes using headgroup aminoconjugates of type **4**.

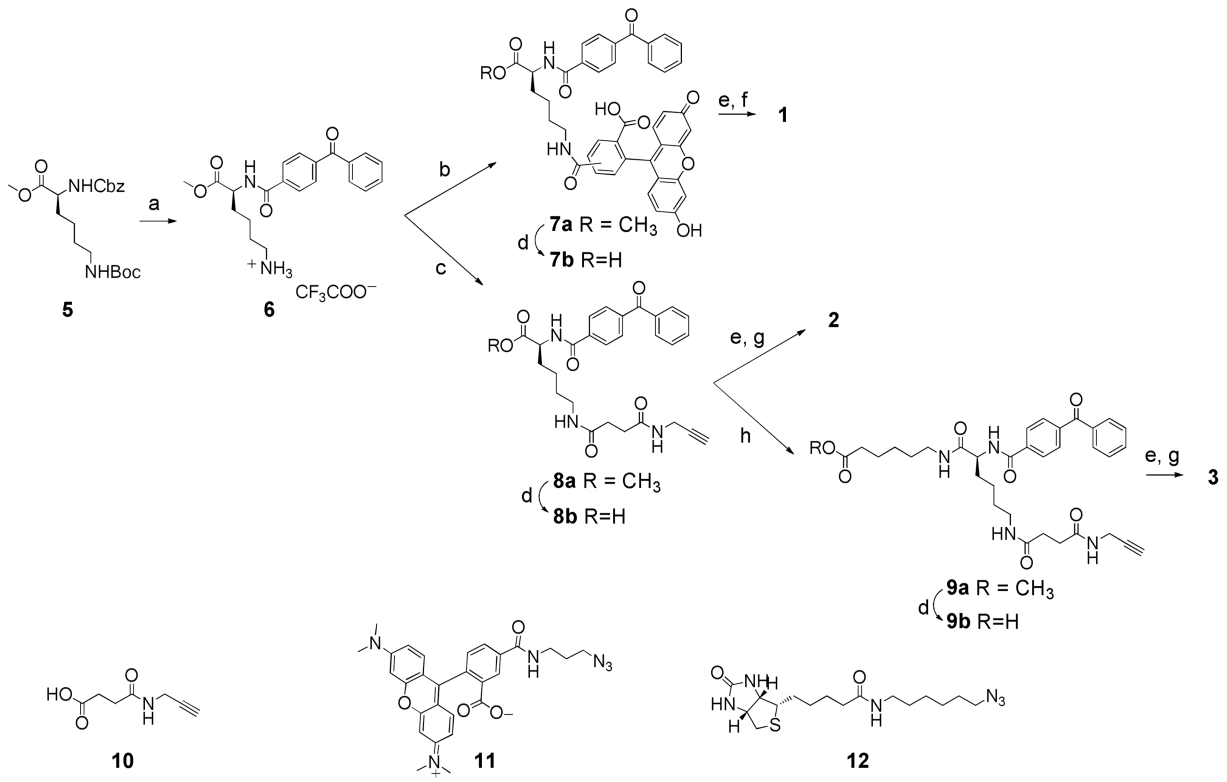

a. i) H_2, Pd/C, MeOH ii) Benzoylbenzoic Acid, EDCI, NMM, DMAP, DMF iii) TFA, CH_2Cl_2; b. EDCI, NMM, DMAP,DMF, 5(6)-carboxy fluorescein; c. **10**, EDCI, NMM, DMAP, MeOH/$CHCl_3$; d. NaOH, MeOH; e. NHS, DCC, THF; f. **4a**, TEAB, DMF, THF; g. **4b**, TEAB, DMF, THF; h.5-aminocaproic acid methyl ester hydrochloride, EDCI, NMM, DMAP, MeOH/$CHCl_3$.

Scheme 2.

Synthesis of bifunctional lysine moieties bearing different secondary tags to generate PIPn activity probes **1**−**3**.

Table 1

Proteins identified from proteomic studies with greater than 5 fold enrichments of spectral counts in probe-labeled samples relative to controls. References are included for those proteins that have been identified in other global proteomic studies.

Accession #	Abbreviation	Protein
P62191	PRS4	26S protease regulatory subunit 4
Q9BWD1	THIC	Acetyl-CoA acetyltransferase, cytosolic
Q99798	ACON	Aconitate hydratase, mitochondrial
P61160	ARP2	Actin-related protein 2
P54819	KAD2	Adenylate kinase 2, mitochondrial
P00568	KAD1	Adenylate kinase isoenzyme 1
P15121	ALDR	Aldose reductase
P12814	ACTN1	Alpha-actinin-1
O43707	ACTN4	Alpha-actinin-4[25]
P04083	ANXA1	Annexin A1
P07355	ANXA2	Annexin A2[25]
P14868	SYDC	Aspartyl-tRNA synthetase, cytoplasmic
P25705	ATPA	ATP synthase subunit alpha, mitochondrial
P06576	ATPB	ATP synthase subunit beta, mitochondrial
P61221	ABCE1	ATP-binding cassette sub-family E member 1
P53396	ACLY	ATP-citrate synthase
P31939	PUR9	Bifunctional purine biosynthesis protein PURH
P11586	C1TC	C-1-tetrahydrofolate synthase, cytoplasmic
P16152	CBR1	Carbonyl reductase [NADPH] 1 OS=Homo sapiens GN=CBR1 PE=1 SV=3
O75828	CBR3	Carbonyl reductase [NADPH] 3
P68400	CSK21	Casein kinase II subunit alpha
P19784	CSK22	Casein kinase II subunit alpha'
Q00610	CLH1	Clathrin heavy chain 1[25]
P53621	COPA	Coatomer subunit alpha[25]
P21399	ACOC	Cytoplasmic aconitate hydratase
Q14204	DYHC1	Cytoplasmic dynein 1 heavy chain 1
P09417	DHPR	Dihydropteridine reductase
O00429	DNM1L	Dynamin-1-like protein
P30084	ECHM	Enoyl-CoA hydratase, mitochondrial
Q14240	IF4A2	Eukaryotic initiation factor 4A-II
P56537	IF6	Eukaryotic translation initiation factor 6
P55060	XPO2	Exportin-2[25]
P49327	FAS	Fatty acid synthase[25]
P21333	FLNA	Filamin-A[25]
P04075	ALDOA	Fructose-bisphosphate aldolase A

Accession #	Abbreviation	Protein
P17931	LEG3	Galectin-3[25]
Q92820	GGH	Gamma-glutamyl hydrolase
Q06210	GFPT1	Glucosamine--fructose-6-phosphate aminotransferase [isomerizing] 1
P11413	G6PD	Glucose-6-phosphate 1-dehydrogenase[25]
P06744	G6PI	Glucose-6-phosphate isomerase
P04406	G3P	Glyceraldehyde-3-phosphate dehydrogenase[25]
P06737	PYGL	Glycogen phosphorylase, liver form
P49915	GUAA	GMP synthase [glutamine-hydrolyzing]
P62826	RAN	GTP-binding nuclear protein Ran
Q9NRV9	HEBP1	Heme-binding protein 1
P12268	IMDH2	Inosine-5'-monophosphate dehydrogenase 2
P02533	K1C14	Keratin, type I cytoskeletal 14
P08779	K1C16	Keratin, type I cytoskeletal 16
P35527	K1C9	Keratin, type I cytoskeletal 9
Q9HA64	KT3K	Ketosamine-3-kinase
P33176	KINH	Kinesin-1 heavy chain[25]
Q04760	LGUL	Lactoylglutathione lyase
P42704	LPPRC	Leucine-rich PPR motif-containing protein, mitochondrial[25]
Q93052	LPP	Lipoma-preferred partner
P40926	MDHM	Malate dehydrogenase, mitochondrial
O95983	MBD3	Methyl-CpG-binding domain protein 3
P26038	MOES	Moesin[25]
P35579	MYH9	Myosin-9[25]
P43490	NAMPT	Nicotinamide phosphoribosyltransferase
P06748	NPM	Nucleophosmin[25]
P15531	NDKA	Nucleoside diphosphate kinase A
P30041	PRDX6	Peroxiredoxin-6
P30086	PEBP1	Phosphatidylethanolamine-binding protein 1
P00558	PGK1	Phosphoglycerate kinase 1
Q9Y617	SERC	Phosphoserine aminotransferase
Q15365	PCBP1	Poly(rC)-binding protein 1
P26599	PTBP1	Polypyrimidine tract-binding protein 1
O60568	PLOD3	Procollagen-lysine,2-oxoglutarate 5-dioxygenase
P48147	PPCE	Prolyl endopeptidase
Q9UL46	PSME2	Proteasome activator complex subunit 2
P61289	PSME3	Proteasome activator complex subunit 3
P28070	PSB4	Proteasome subunit beta type-4
Q99497	PARK7	Protein DJ-1
Q92597	NDRG1	Protein NDRG1

Accession #	Abbreviation	Protein
P31150	GDIA	Rab GDP dissociation inhibitor alpha
P35241	RADI	Radixin
P46940	IQGA1	Ras GTPase-activating-like protein IQGAP1[25]
Q15019	SEP3	Septin-2[25]
P34897	GLYM	Serine hydroxymethyltransferase, mitochondrial
P30153	2AAA	Serine/threonine-protein phosphatase 2A 65 kDa regulatory subunit A alpha isoform
P02768	ALBU	Serum albumin
Q13813	SPTA2	Spectrin alpha chain, brain[25]
P17987	TCPA	T-complex protein 1 subunit alpha
P50991	TCPD	T-complex protein 1 subunit delta
Q99832	TCPH	T-complex protein 1 subunit eta
P50990	TCPQ	T-complex protein 1 subunit theta
P40227	TCPZ	T-complex protein 1 subunit zeta
Q8NBS9	TXND5	Thioredoxin domain-containing protein 5
P23193	TCEA1	Transcription elongation factor A protein 1
Q92616	GCN1L	Translational activator GCN1[25]
P23381	SYWC	Tryptophanyl-tRNA synthetase, cytoplasmic
P30085	KCY	UMP-CMP kinase
Q16831	UPP1	Uridine phosphorylase 1
P38606	VATA	V-type proton ATPase catalytic subunit A
P21281	VATB2	V-type proton ATPase subunit B, brain isoform
P49748	ACADV	Very long-chain specific acyl-CoA dehydrogenase, mitochondrial[25]
P13010	XRCC5	X-ray repair cross-complementing protein 5

Table 2

Proteins identified from proteomic studies with between 2-5 fold enrichments of spectral counts in probe-labeled samples relative to controls. References are included for those proteins that have been identified in other global proteomic studies.

P61604	CH10	10 kDa heat shock protein, mitochondrial
P31946	1433B	14-3-3 protein beta/alpha
Q04917	1433F	14-3-3 protein eta
P61981	1433G	14-3-3 protein gamma
P43686	PRS6B	26S protease regulatory subunit 6B
P62195	PRS8	26S protease regulatory subunit 8
Q99460	PSMD1	26S proteasome non-ATPase regulatory subunit 1
Q6NVY1	HIBCH	3-hydroxyisobutyryl-CoA hydrolase, mitochondrial
P62841	RS15	40S ribosomal protein S15
P08708	RS17	40S ribosomal protein S17
P15880	RS2	40S ribosomal protein S2
P23396	RS3	40S ribosomal protein S3
P61247	RS3A	40S ribosomal protein S3a
P62081	RS7	40S ribosomal protein S7
P46781	RS9	40S ribosomal protein S9
Q5TFE4	NT5D1	5'-nucleotidase domain-containing protein 1
P17858	K6PL	6-phosphofructokinase, liver type[25]
P08237	K6PF	6-phosphofructokinase, muscle type
P10809	CH60	60 kDa heat shock protein, mitochondrial
P46778	RL21	60S ribosomal protein L21
P62750	RL23A	60S ribosomal protein L23a
P36578	RL4	60S ribosomal protein L4
P46777	RL5	60S ribosomal protein L5
P62424	RL7A	60S ribosomal protein L7a
P11021	GRP78	78 kDa glucose-regulated protein
P24752	THIL	Acetyl-CoA acetyltransferase, mitochondrial
O15144	ARPC2	Actin-related protein 2/3 complex subunit 2
O15145	ARPC3	Actin-related protein 2/3 complex subunit 3
P55263	ADK	Adenosine kinase
P49588	SYAC	Alanyl-tRNA synthetase, cytoplasmic
P61163	ACTZ	Alpha-centractin
P08133	ANXA6	Annexin A6
Q9BZZ5	API5	Apoptosis inhibitor 5
Q96P48	ARAP1	Arf-GAP with Rho-GAP domain, ANK repeat and PH domain-containing protein 1[30]
P54136	SYRC	Arginyl-tRNA synthetase, cytoplasmic
P08243	ASNS	Asparagine synthetase [glutamine-hydrolyzing]

Q13057	COASY	Bifunctional coenzyme A synthase
P27797	CALR	Calreticulin
O43852	CALU	Calumenin
O00299	CLIC1	Chloride intracellular channel protein 1[25]
Q9Y696	CLIC4	Chloride intracellular channel protein 4
Q00610	CLH1	Clathrin heavy chain 1[25]
P53621	COPA	Coatomer subunit alpha[25]
Q07021	C1QBP	Complement component 1 Q subcomponent-binding protein, mitochondrial
P04080	CYTB	Cystatin-B
Q9UHD1	CHRD1	Cysteine and histidine-rich domain-containing protein 1
P28838	AMPL	Cytosol aminopeptidase
O00154	BACH	Cytosolic acyl coenzyme A thioester hydrolase
Q96KP4	CNDP2	Cytosolic non-specific dipeptidase
P54886	P5CS	Delta-1-pyrroline-5-carboxylate synthase
P15924	DESP	Desmoplakin
Q16555	DPYL2	Dihydropyrimidinase-related protein 2
P28340	DPOD1	DNA polymerase delta catalytic subunit
P49736	MCM2	DNA replication licensing factor MCM2
P31689	DNJA1	DnaJ homolog subfamily A member 1
Q9H223	EHD4	EH domain-containing protein[25]
P13804	ETFA	Electron transfer flavoprotein subunit alpha, mitochondrial
P13639	EF2	Elongation factor 2
P49411	EFTU	Elongation factor Tu, mitochondrial
P60842	IF4A1	Eukaryotic initiation factor 4A-I
P62495	ERF1	Eukaryotic peptide chain release factor subunit 1
P60228	EIF3E	Eukaryotic translation initiation factor 3 subunit E
Q15056	IF4H	Eukaryotic translation initiation factor 4H
P63241	IF5A1	Eukaryotic translation initiation factor 5A-1
P49327	FAS	Fatty acid synthase[25]
O75369	FLNB	Filamin-B[25]
P39748	FEN1	Flap endonuclease 1
P07954	FUMH	Fumarate hydratase, mitochondrial
P17931	LEG3	Galectin-3[25]
Q13630	FCL	GDP-L-fucose synthase
P06396	GELS	Gelsolin[24]
O94925	GLSK	Glutaminase kidney isoform, mitochondrial
Q9Y2Q3	GSTK1	Glutathione S-transferase kappa 1
P21266	GSTM3	Glutathione S-transferase Mu 3
P04406	G3P	Glyceraldehyde-3-phosphate dehydrogenase[25]
P11216	PYGB	Glycogen phosphorylase, brain form

P08238	HS90B	Heat shock protein HSP 90-beta
Q14103	HNRPD	Heterogeneous nuclear ribonucleoprotein D0
P52597	HNRPF	Heterogeneous nuclear ribonucleoprotein F
P61978	HNRPK	Heterogeneous nuclear ribonucleoprotein K
P26583	HMGB2	High mobility group protein B2
Q16836	HCDH	Hydroxyacyl-coenzyme A dehydrogenase, mitochondrial
Q9UI26	IPO11	Importin-11
P50213	IDH3A	Isocitrate dehydrogenase [NAD] subunit alpha, mitochondrial
P26440	IVD	Isovaleryl-CoA dehydrogenase, mitochondrial
P14923	PLAK	Junction plakoglobin
P08779	K1C16	Keratin, type I cytoskeletal 16
P35527	K1C9	Keratin, type I cytoskeletal 9
P04264	K2C1	Keratin, type II cytoskeletal 1
P35908	K22E	Keratin, type II cytoskeletal 2 epidermal
P33176	KINH	Kinesin-1 heavy chain[25]
P07195	LDHB	L-lactate dehydrogenase B chain
Q32MZ4	LRRF1	Leucine-rich repeat flightless-interacting protein 1
Q8N1G4	LRC47	Leucine-rich repeat-containing protein 47
O60711	LPXN	Leupaxin
P40925	MDHC	Malate dehydrogenase, cytoplasmic
Q9UNF1	MAGD2	Melanoma-associated antigen D2
Q15691	MARE1	Microtubule-associated protein RP/EB family member 1[25]
P28482	MK01	Mitogen-activated protein kinase 1[25]
P60660	MYL6	Myosin light polypeptide 6[25]
O00159	MYO1C	Myosin-Ic
P51606	RENBP	N-acylglucosamine 2-epimerase
Q14697	GANAB	Neutral alpha-glucosidase AB
Q15233	NONO	Non-POU domain-containing octamer-binding protein
Q8TAT6	NPL4	Nuclear protein localization protein 4 homolog
P12270	TPR	Nucleoprotein TPR
Q8WXF1	PSPC1	Paraspeckle component 1
P62937	PPIA	Peptidyl-prolyl cis-trans isomerase A
Q13526	PIN1	Peptidyl-prolyl cis-trans isomerase NIMA-interacting 1
Q13162	PRDX4	Peroxiredoxin-4[30]
Q9Y2H2	SAC2	Phosphatidylinositide phosphatase SAC2
Q13492	PICAL	Phosphatidylinositol-binding clathrin assembly protein[24]
Q15149	PLEC	Plectin
Q6P2Q9	PRP8	Pre-mRNA-processing-splicing factor 8
Q99471	PFD5	Prefoldin subunit 5
P02545	LMNA	Prelamin-A/C

P26196	DDX6	Probable ATP-dependent RNA helicase DDX6
P28066	PSA5	Proteasome subunit alpha type-5
P20618	PSB1	Proteasome subunit beta type-1
P49720	PSB3	Proteasome subunit beta type-3
P28072	PSB6	Proteasome subunit beta type-6
Q99436	PSB7	Proteasome subunit beta type-7
P28062	PSB8	Proteasome subunit beta type-8
P28065	PSB9	Proteasome subunit beta type-9
P30101	PDIA3	Protein disulfide-isomerase A3
P07237	PDIA1	Protein disulfide-isomerase
Q9NUQ9	FA49B	Protein FAM49B
P22061	PIMT	Protein-L-isoaspartate(D-aspartate) O-methyltransferase
Q9NVS9	PNPO	Pyridoxine-5'-phosphate oxidase
P50395	GDIB	Rab GDP dissociation inhibitor beta
P31153	METK2	S-adenosylmethionine synthase isoform type-2
P10768	ESTD	S-formylglutathione hydrolase
Q16181	SEP3	Septin-7[25]
Q9UHD8	SEP10	Septin-9[25]
Q13501	SQSTM	Sequestosome-1
P63151	2ABA	Serine/threonine-protein phosphatase 2A 55 kDa regulatory subunit B alpha Isoform[25]
Q15257	PTPA	Serine/threonine-protein phosphatase 2A activator
P62136	PP1A	Serine/threonine-protein phosphatase PP1-alpha catalytic subunit[25]
P50454	SERPH	Serpin H1[30]
Q01082	SPTB2	Spectrin beta chain, brain 1[25]
Q15637	SF01	Splicing factor 1
Q13435	SF3B2	Splicing factor 3B subunit 2
Q15393	SF3B3	Splicing factor 3B subunit 3
P26368	U2AF2	Splicing factor U2AF 65 kDa subunit
P31948	STIP1	Stress-induced-phosphoprotein 1
Q9UH65	SWP70	Switch-associated protein 70[30]
Q99536	VAT1	Synaptic vesicle membrane protein VAT-1 homolog
P78371	TCPB	T-complex protein 1 subunit beta
P48643	TCPE	T-complex protein 1 subunit epsilon
P49368	TCPG	T-complex protein 1 subunit gamma
O95881	TXD12	Thioredoxin domain-containing protein 12
Q15645	TRP13	Thyroid receptor-interacting protein 13
P20290	BTF3	Transcription factor BTF3
Q8WXI9	P66B	Transcriptional repressor p66-beta
Q9Y5L0	TNPO3	Transportin-3

P22102	PUR2	Trifunctional purine biosynthetic protein adenosine-3
P60174	TPIS	Triosephosphate isomerase
P23381	SYWC	Tryptophanyl-tRNA synthetase, cytoplasmic
P07437	TBB5	Tubulin beta chain
P04350	TBB4	Tubulin beta-4 chain
Q6IBS0	TWF2	Twinfilin-2
O15042	SR140	U2-associated protein SR140
Q93009	UBP7	Ubiquitin carboxyl-terminal hydrolase 7
P61088	UBE2N	Ubiquitin-conjugating enzyme E2 N^{25}
Q04323	UBXN1	UBX domain-containing protein 1
P54727	RD23B	UV excision repair protein RAD23 homolog B
P50552	VASP	Vasodilator
Q9NQW7	XPP1	Xaa